BNL-225497-2024-JAAM

Diversifying self-assembled phases in block copolymer thin films via blending

G. . Doerk

To be published in "Physical Review Materials"

December 2023

Center for Functional Nanomaterials

Brookhaven National Laboratory

U.S. Department of Energy

USDOE Office of Science (SC), Basic Energy Sciences (BES). Scientific User Facilities (SUF)

DISCLAIMER

Research Updates

Diversifying self-assembled phases in block copolymer thin films via blending

Gregory S. Doerk* and Kevin G. Yager†
Center for Functional Nanomaterials, Brookhaven National Laboratory, Upton, New York 11973, USA

(Received 28 August 2023; accepted 14 November 2023; published 8 December 2023)

Block copolymer (BCP) thin films readily self-assemble into intricate nanoscale morphologies, with structure dictated by chain architecture. As the field searches for more control over structure formation, it is natural to investigate more sophisticated control mechanisms, such as synthesizing more complex chain architectures or applying directing fields. We review the use of a simple but powerful method for controlling self-assembly: blending of BCPs with homopolymers or other BCPs. Blending enables tailoring ordering kinetics, the spatial distribution of chains throughout the film thickness, and the nanoscale morphology itself. Blending is thus emerging as a remarkably simple and powerful means of tailoring self-assembled morphologies.

DOI: 10.1103/PhysRevMaterials.7.120301

I. INTRODUCTION

Inspired by its ubiquity in the natural world, self-assembly has long appealed to materials scientists as a paradigm for precisely and inexpensively controlling hierarchical nanoscale material structure across macroscale dimensions. Block copolymers (BCPs), macromolecules whose chemistry varies in a defined manner based on the molecular architecture, are a canonical self-assembling nanomaterial [1–3]. The simplest BCP exemplars—linear BCPs consisting of two or more chemically distinct polymer chains—have attracted interest in their self-assembly behavior since their introduction in the mid-20th century. Though much of the research on BCP self-assembly has been devoted to bulk systems, the impressive progress of the microelectronics industry and its demand for continuous improvements in nanopatterning resolution has driven intense research in exploiting the precise nanomorphology control possible in BCP thin films to push the limits of lithographic patterning via directed self-assembly [4–12]. Other emerging applications such as isoporous membrane synthesis [13–17], nanophotonic light management [18–24], and surface wettability control [25–28] highlight the immense value of large-area, cost-effective nanopatterning that is made possible through thin film BCP nanopatterning.

Fully leveraging the potential of thin film BCP self-assembly hinges both upon expanding the range of available self-assembled nanopatterns and realizing greater flexibility to customize these patterns according to application needs. Substantial progress has been achieved through the synthesis of BCPs with more complex chemistries and chain architectures [29–31]. Other lines of research use nontrivial sample preparation methods to yield structures from existing materials [29]. One powerful strategy is to tune assembly behavior by formulating blends. Blending polymers sidesteps challenges of time and cost that sometimes accompany polymer synthesis but introduces added complexity based on new degrees of freedom associated with the blended additives. In this mini-review, we highlight selected research on self-assembling polymer blend thin films and distill basic principles that may guide further research in this area. We first discuss key concepts that may be used to understand self-assembly in blends of BCPs with homopolymers (HPs) and other BCPs. We then describe advanced methods which improve and accelerate our ability to characterize polymer blend assembly, and we summarize recent demonstrations of complex morphological control in self-assembled polymer blend thin films. We then lay out guiding principles and design rules for interpreting and directing the self-assembly of polymer blends, especially as pertinent to thin films. Finally, we conclude with our perspectives on future directions for research in this area.

II. BCP/HP BLENDS

A basic understanding about the self-assembly behavior of BCPs blended with HPs is provided by Flory-Huggins solution theory, which quantitatively describes the change in normalized molar Gibbs free energy ($\Delta G/RT$) from blending two HPs. Assuming that the monomer units of polymers A and B occupy the same reference volume, the theory can be summarized by [32]

$$\frac{\Delta G}{RT} = \frac{\phi_A}{N_A}\ln\phi_A + \frac{\phi_B}{N_B}\ln\phi_B + \chi\phi_A\phi_B. \quad (1)$$

Here, R is the universal gas constant, T is absolute temperature, N_i and ϕ_i are the degree of polymerization and volume fraction of the ith polymer (i = A or B), respectively, and χ is the Flory-Huggins interaction parameter, which quantifies the change in Gibbs free energy due to pairwise segmental interactions. The first two terms in Eq. (1) arise due to

*gdoerk@bnl.gov
†kyager@bnl.gov

the combinatorial entropy of mixing, while the third term primarily represents the enthalpic change due to segmental pair interactions. Cursory inspection indicates that the large degree of polymerization for most polymers reduces the relative entropic contribution from mixing, rendering chemical compatibility (i.e., the magnitude and sign of χ) the dominant factor dictating phase behavior. For chemically incompatible polymers, intrinsic immiscibility drives macrophase separation. The covalent linkage in BCPs counteracts macrophase separation, leading to the formation of nanoscale morphologies in pure BCP systems. The covalent connection between two chemically distinct polymers also enables BCPs to act as compatibilizers for otherwise immiscible HP blends. Research in the mid- to late 20th century therefore featured many reports on the assembly behavior of bulk BCP/HP blends [33–48]. There is sustained interest in this topic, with recent research uncovering puzzles about the competing influences of chemical repulsion and chain connectivity in polymer blends with BCPs and the corresponding nuanced effect on self-assembling behavior [49–58]. Myriad nanoscale morphologies have been found to assemble based on mixture composition, component characteristics (molar mass, chain architecture, segmental stiffness, etc.), and processing conditions.

In general, a HP with significant segregation strength with respect to all blocks in a BCP will macrophase separate from the BCP for the same reasons as two incompatible HPs would. For this reason, significant attention has been devoted to athermal blends of BCPs with chemically alike HPs. For diblock copolymers with A and B blocks (shorthand AB), these include binary (AB/A or AB/B) and ternary (AB/A/B) blends. The chemical equivalence of the blended HPs introduces no new interaction terms, and so their distribution with respect to the BCP domains and their impact on the assembly behavior has been mainly attributed to entropic effects. Relative chain length is of central importance in characterizing the phase behavior in athermal blends, parameterized in AB/A binary blends, for example, by the ratio of the A HP chain length to the length of the A block in AB or $\alpha = N_{AH}/N_A$. In this framework, binary blend assembly behavior has been classified in three regimes. For $\alpha \gg 1$, the HP occupies too much volume to be solubilized by the BCP, resulting in macrophase separation [Fig. 1(a)]. When the HP chain length is similar to the corresponding block ($\alpha \sim 1$), the blend is considered to fall within the *dry brush* regime, wherein the HP is solubilized by the BCP but is localized to the interior of the self-assembled domains to maximize conformational entropy for both HP and BCP chains [Fig. 1(b)]. The name is derived from the similarity between polymer brushes grafted to surfaces and the block chains extending from domain interfaces, where these block brushes are dry in the sense that the HP chains do not penetrate them. In contrast, blends in which $\alpha < 1$ are said to be in a *wet brush* regime, where HP distributes uniformly within the domains in which it resides [Fig. 1(c)], allowing it to maximize translational entropy without significant loss of conformational entropy.

The statistical degree of HP localization scales proportionally with α and has important implications for stabilizing complex morphologies in binary blends, in some cases with reduced symmetry [36,40,42,44,47,49–51,56]. As an example, Winey *et al.* [46] demonstrated that an ordered

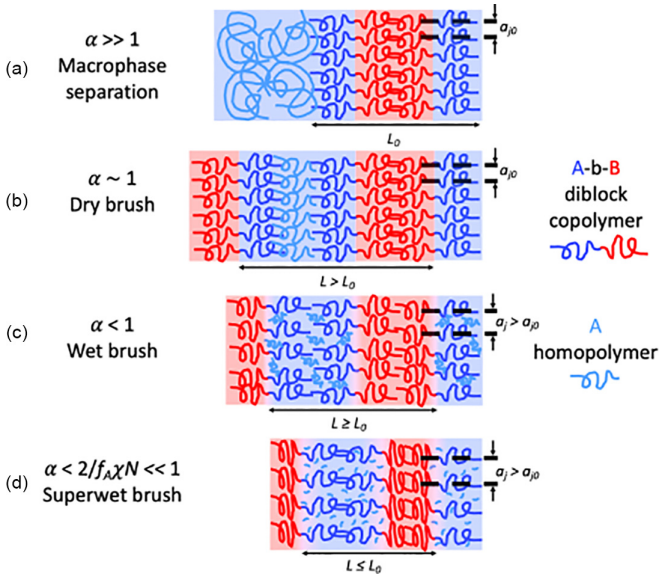

FIG. 1. Regimes for binary diblock copolymer/homopolymer (HP) blend self-assembly. (a) At values for the ratio of degrees of polymerization of the HP to the chemically compatible polymer block $\gg 1$ ($\alpha \gg 1$), the HP cannot be solubilized, and the blend separates into block copolymer (BCP)-rich and HP-rich phases. The BCP domain spacing (L) and area per junction at the domain interface (a_j) are nominally unchanged from their equilibrium values, L_0 and a_{j0}, respectively. (b) In the dry brush regime ($\alpha \sim 1$), the HP is solubilized within its like domain but localizes to the domain center. L is increased, but a_{j0} is unchanged. (c) In the wet brush regime ($\alpha < 1$), HP distributes more uniformly within the domain to maximize translational entropy, without significant loss in conformational entropy. Domain swelling with HP increases L, but this is in part counteracted by the increased a_j that causes opposing block chains to contract due to compressibility. (d) In the superwet brush regime ($\alpha < \sim 2/f_A\chi N \ll 1$), very short HPs distribute uniformly throughout the domain and up to the domain interface. There, they screen the block interactions, allowing BCP chains that are normally stretched at the interface to relax. The result is a decrease in L to less than L_0.

bicontinuous phase assembled at specific weight fractions of polystyrene (PS) HP blended with PS-*block*-polyisoprene (PS-*b*-PI) BCP only for values of α from ~0.2 to ~0.9. In this range, the addition of HP yields the domain interfacial curvature required for a bicontinuous phase, while at least a portion of the HP localizes to interstices, alleviating packing frustration and the associated entropic penalties due to chain stretching [40]. More recently, the role of HP distribution in bulk athermal AB/A blends has been recognized in stabilizing Frank-Kasper phases (A15, σ, and C14 and C15 Laves phases) with complex spherical packing [55,59–64]. The HP redistributes within the morphology in nontrivial ways to relieve packing frustration [62–64], with varying optimal α values in the range of $\leqslant 1$ depending on whether the HP resides in the minority [55] or majority phase [60].

The capacity for blended HP to distribute within self-assembled domains to compensate for BCP packing frustration and chain stretching/compression leads to interesting structure formation in thin films. The interplay of HP redistribution with film boundary conditions and strong confinement

leads to significant changes in the self-assembled morphologies. A hard substrate breaks the bulk lattice symmetry, enforcing a tendency toward assembled morphologies with ideal two-dimensional (2D) packing symmetry over a representative decay length in the confinement direction [65]. As an example, symmetry breaking for films of silicon-supported PS-block-poly(2-vinylpyridine) (PS-*b*-P2VP) spheres leads to a discontinuous transition from hexagonal to face-centered orthorhombic (FCO) packing, followed by a gradual deformation to body-centered cubic (BCC) packing with a substrate-parallel (110) plane as film thickness is increased [66]. Adding as little as 2% (w/w) of relatively short PS HP ($\alpha \sim 0.22$) that can localize in part to interstices between spheres, however, conspicuously increases the thickness and breadth of the hexagonal/FCO transition [Fig. 2(a)] [57]. Thickness-dependent transitions from a bulk gyroid morphology to thin film hexagonally perforated lamellae (HPL) [67] have been observed in bulk gyroid-forming AB/A blends as well [68], though differences in the transition thickness between neat and blend systems have not been investigated.

At the lower limit of the wet brush regime ($\alpha \ll 1$), the highly uniform distribution of HP within their solubilized domains has striking effects on the stability of domains, the kinetics of self-assembly, and the range of accessible morphologies. In athermal binary diblock and triblock copolymer blends with HP, the uniform HP distribution increases the area per BCP chain at domain interfaces [Fig. 1(d)]; incompressibility requires the opposing BCP chain in the opposing block to contract to fill space, ultimately leading to a reduction in overall domain spacing that has been observed both in the bulk [47] and in thin films [51,58,69–72]. This uniformly distributed HP, also present in ternary blends (e.g., AB/A/B) with $\alpha \ll 1$, screens interactions between BCP chains of opposing blocks and therefore acts as a BCP diluent, like solvents [40]. This screening weakens the domain interface, broadening the interfacial width and potentially destabilizing the morphology entirely. On the other hand, it also lowers diffusive energy barriers in the microphase separated state, which dramatically accelerates assembly kinetics. We have previously shown that blending PS and poly(methyl methacrylate) (PMMA) HP with PS-*b*-PMMA BCPs can increase ordering kinetics in thin films by an order of magnitude [69] [Fig. 2(b)], accelerates domain reorientation in cylindrical-forming films more than a monolayer thick [70], and enables assembly of thin film patterns with 100–300 nm scale periodicity using ultrahigh molecular weight (UHMW) BCPs (>500 kg/mol) in practical time periods, e.g., 1 h [73].

Based on the significant changes in assembly behavior in blends when $\alpha \ll 1$ in comparison with more conventional wet brush BCP/HP blends, we can propose a fourth regime of *superwet brush* blends. It is worthwhile to discuss how one might demarcate the transition between wet and superwet brush regimes. In conventional wet brush blends, though the HP distributes fairly uniformly throughout its solubilizing domain, increasing volume fractions of HP increases the domain spacing and eventually results in macrophase separation. On the other hand, in superwet brush blends, increasing HP volume fraction decreases the domain spacing and eventually destabilizes any phase separated morphology. Though treated more rigorously in early calculations by Vavasour and

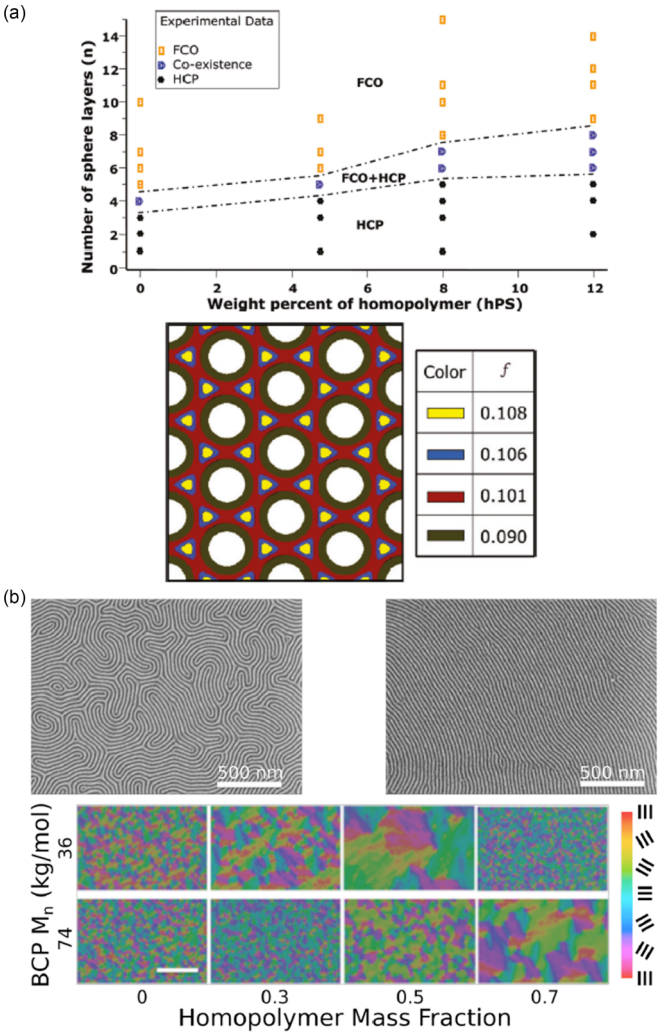

FIG. 2. Exemplary phase behavior of block copolymer (BCP)/homopolymer (HP) blend thin films. (a) Top: Phase diagram for blends of polystyrene (PS) HP with sphere-forming PS-block-poly(2-vinylpyridine)(PS-*b*-P2VP) BCP as a function of film thickness and HP weight fraction. The addition of PS HP increases and broadens the transition from hexagonal close-packed (HCP) to face-centered orthorhombic (FCO) sphere packing with film thickness. Bottom: Self-consistent field theory calculations show that this behavior can be explained by the localization of PS HP to interstices between spheres, which reduces energy penalties due to chain stretching experienced by the neat BCP. Adapted with permission from Ref. [57]. Copyright 2010, American Chemical Society. (b) Accelerated assembly kinetics in PS-block-poly(methyl methacrylate) (PS-*b*-PMMA)/PS/PMMA thin films. Top: Scanning electron microscope (SEM) images of lamellar nanopatterns formed by assembly of a symmetric 36 kg/mol neat PS-*b*-PMMA thin film (left) and its counterpart thin film isoplethic ternary blend with 50% (w/w) ~3 kg/mol PS and PMMA HP (right). The neat BCP exhibits much smaller pattern grains, though the films were annealed under the same conditions. Bottom: False-colored orientation maps showing kinetic enhancement as a function of ~3 kg/mol HP mass fraction for thin film ternary blends with symmetric 36 and 74 kg/mol PS-*b*-PMMA. Reduced color variation indicates larger pattern grains. This kinetic enhancement can be attributed in part to screening of BCP interactions by the very short blended HP. Adapted with permission from Ref. [69]. Copyright 2017, American Chemical Society.

Whitmore [52], a simple estimate for the value of α that separates these regimes can be obtained heuristically based on the work of Broseta and Fredrickson [34] on athermal, symmetric ternary AB/A/B blends along the isopleth (i.e., in which the HP composition matches the block volume fractions). Using their analytical expression for the location of the Lifshitz tricritical point separating disordered (mixed), macrophase separated, and microphase separated regions, one may note that increasing HP fraction only leads to a disordered phase when the segregation strength of the Lifshitz point (χN_{Lifshitz}) is greater than that of the neat BCP (χN). Straightforward algebra reveals that a superwet brush regime is entered when $\alpha <\sim 2/f_A\chi N$ [69], where f_A is the volume fraction of A blocks. Note, we have written this criterion in a form that is consistent with the definition of α presented earlier in this review. Intuitively, this result may be expected naturally, as it coincides with the critical point for a symmetric, binary polymer blend ($\chi N_H < 2$), below which HP phase separation will not occur [32]. Still, this analysis shows that, even in athermal blends, the distribution of HP within its solubilizing domain is influenced by its enthalpic interactions with the polymers in the opposing domains.

Athermal wet brush HPs can have pronounced effects on the self-assembled morphology in very thin films ($\sim$1 L_0 thick) as a result of domain confinement and chain enrichment at film surfaces. The HPs in the blend, which are notably shorter than the BCPs, can enrich both the film substrate and free surfaces based on surface tension differences and an entropic attraction for chain ends to film surfaces that promotes surface enrichment of short HPs [74–76]. This HP surface enrichment can create a wetting layer that drives domain reorientation [72]. This reorientation is opposed in highly confined submonolayer films ($<$1 L_0 thick), however, by steep entropic penalties due to the required BCP chain stretching, as shown by molecular dynamics (MD) simulations in Fig. 3(a). MD simulations performed for film thickness just above a monolayer, in which this entropic penalty from film confinement is reduced, reveal that surface enrichment changes the domain orientation and relative composition of the film interior [Fig. 3(b)], a finding that is corroborated by experiments on blend films of PS-*b*-PMMA with very short ($\sim$1 kg/mol) PS and PMMA HPs of varying thickness [Fig. 3(c)]. This surface enrichment-driven polymer redistribution likely has unknown implications for the morphology and domain spacing in many BCP/HP blend thin films.

Though athermal blends have received significant attention, blending AB BCPs with C HPs having selective favorable interactions with the B block through strongly attractive interactions introduces ways to engineer the assembled morphology. For instance, a strong hydrogen-bonding interaction causes the C HP to distribute uniformly throughout the B domain, acting in some ways like a superwet brush HP ($\alpha \ll 1$). This can cause the domain spacing to decrease with increasing C HP volume fraction due to increased area per BCP chain, whereas an AB/B blend with B HP of comparable molar mass exhibits increasing domain spacing with increasing HP fraction [77]. It should be noted, however, that domain spacing can increase upon C HP addition for weakly attractive B-C hydrogen-bonding interactions [78] or in cases where $\chi_{AC} > \chi_{AB}$ [79]. Moreover, with strongly attractive

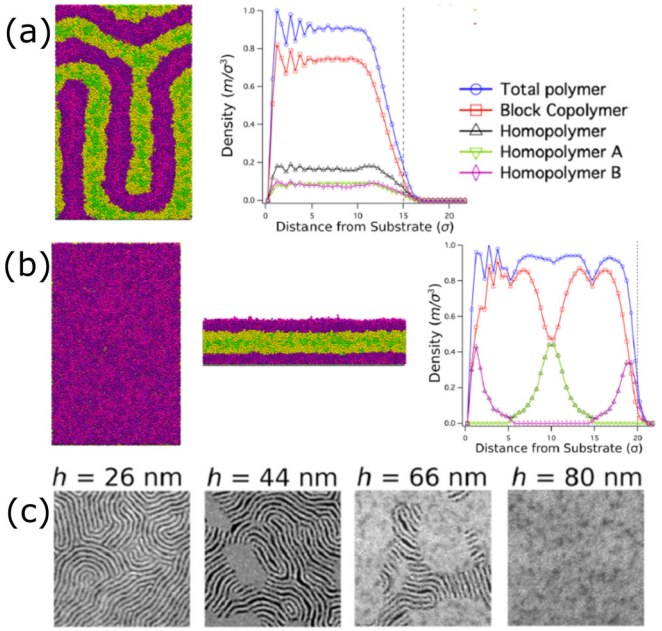

FIG. 3. Athermal block copolymer (BCP)/homopolymer (HP) blend domain reorientation in thin films resulting from HP surface enrichment. (a) A top-view coarse grained molecular dynamics (CGMD) simulation snapshot (left) and through-film polymer average density profiles (right) show that vertical orientation is unperturbed for symmetric, isoplethic ternary BCP/HP blends with 20% HP $<$1 L_0 thick. (b) Top-view (left) and cross-section (middle) CGMD snapshots and through-film polymer average density profiles (right) reveal that domains reorient in blend films with the same composition $>$1 L_0 thick. This thickness dependence is not observed for the neat diblock copolymer. (c) Top-view scanning electron microscope (SEM) images of lamellar nanopatterns assembled from ternary blends comprising 60% 75 kg/mol symmetric polystyrene-block-poly(methyl methacrylate) (PS-*b*-PMMA) and 20% each of $\sim$1 kg/mol PS and PMMA for various film thicknesses (h). The increased areal fraction of patches, identified as horizontal lamellae, for $h > L_0$ ($\sim$38 nm) is consistent with the CGMD predictions. Adapted with permission from Ref. [72]. Copyright 2021, American Chemical Society.

B-C hydrogen-bonding interactions, increasing C HP fraction does not destabilize the domain morphology or lead to macrophase separation as in wet brush AB/B blends; instead, the C HP solubilizes readily in the B domain, changing domain interfacial curvature to an extent that is determined by the strength of the attractive B-C interaction [77,80,81]. As shown experimentally by Chen *et al.* [77], stronger attraction substantially alters the domain interfacial curvature, enabling traversal across common ordered phases observed in BCPs (e.g., spheres, cylinders, gyroids, lamellae). In contrast, weaker attractions tend to distort the BCP morphology [77,82]. Surprisingly, strongly attractive hydrogen-bonding interactions can prevent macrophase separation even for dry brush blends ($N_{CH} > N_B$), resulting in order-order transitions like the cases with much shorter C HP [81].

Hydrogen bonding may also be used to selectively incorporate small molecules into one block, generating artificial comb-coil BCPs with hierarchical structure, with a morphol-

ogy having a larger period (∼10+ nm) determined by the BCP supramolecule and a second morphology within the hydrogen-bonding domain having a smaller period (<10 nm) determined by the comb structure [83,84]. These hierarchical assemblies are strongly influenced by processing conditions and may sometimes be switched reversibly between two states by thermal [85,86] or solvent vapor treatment [87–89] as a result of the high entropic energy gain experienced when the small molecules are unbound.

III. BCP BLENDS

Though the thermodynamics driving forces for BCP blends are in principle the same as those that control self-assembly in BCP/HP blends, the additional covalent bond in athermal AB/AB diblock copolymer blends pins the chemical junctions of both components to domain interfaces, introducing an additional element of frustration by preventing localization of either component to domain centers. The simplest case is when the AB volume fractions are similar between the two diblock copolymers. The alike BCPs are well mixed when BCP molecular weights are not too dissimilar, making it possible to tune the domain spacing by varying blend composition. For significant differences in BCP chain lengths, substantial stretching of short chains and compression of long chains entailed by mixing drives macrophase separation between short and long BCP rich phases [90,91].

Blends of chemically alike AB BCPs with sufficiently different A volume fractions (i.e., where each neat BCP assembles into different bulk morphologies) generally assemble into a single phase; they may, however, exhibit coexisting morphologies in some cases. The emergence of coexistence phases in BCP blends can be rationalized in terms of the relative energies of competing states [92]. In traditional (single-component) BCP assembly in the bulk, a single canonical morphology forms that minimizes penalties such as interpenetration of blocks and interfacial curvature. In appropriate blends, multiple morphological motifs may have similar energies, allowing the appearance of coexisting mixtures of these structures. Ultimately, this behavior must be due to the underlying chains. In the case of blends, the two distinct chain types give rise to an additional degree of freedom: the spatial redistribution of chains. Chain-level BCP phenomena can be studied explicitly using coarse-grained MD simulations, wherein BCP chains are modeled as beads connected by springlike interaction potentials [93–97]. MD simulations of blends of cylinder-forming (C) and lamellae-forming (L) BCP chains reproduced the formation of a coexistence of dot and line morphological objects, while confirming the supposition that the underlying chains are distributed roughly homogeneously [96]. That is, both the dot regions (akin to hexagonally packed cylinders) and the line regions (akin to alternating lamellae) are composed of both C and L chains.

Despite this homogeneous chain mixing across large and intermediate scales, notable deviations can be observed at more local scales [Fig. 4(a)]. There are statistical deviations from the average composition at the scale of the individual morphological objects, with dot objects having a slight excess of C chains and line objects having an excess of L chains. Furthermore, the chains redistribute within the morphological

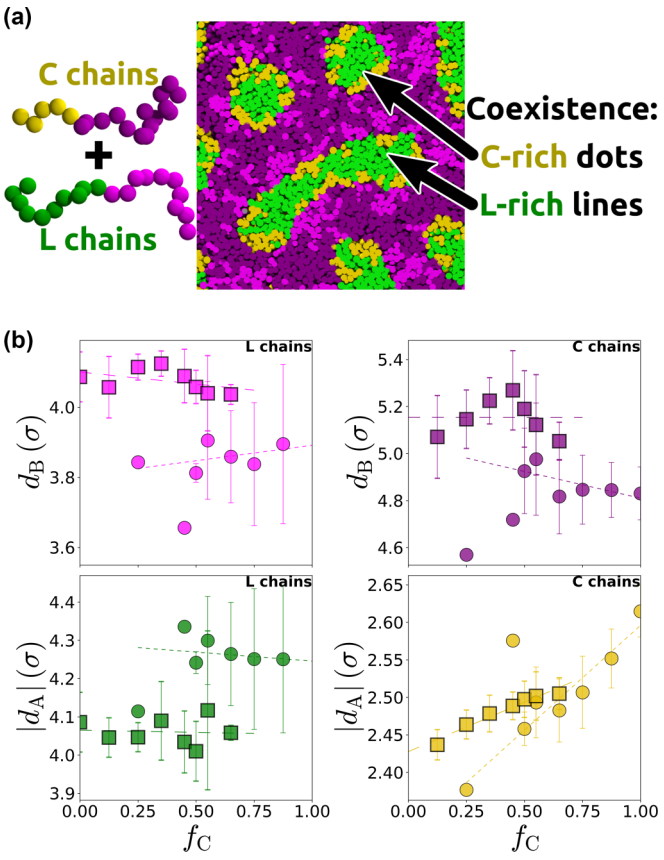

FIG. 4. Coarse-grained molecular dynamics simulations were used to study chain-level effects in block copolymer (BCP) blends. (a) Coexistence phases arise from the underlying cylinder-forming (C) and lamellae-forming (L) chains mixing, while also distributing locally to stabilize the formation of coexisting dot and line objects. (b) Measuring the chain extension (d) within the majority (d_B) and minority (d_A) blocks, as a function of blend composition (f_C), demonstrates that chains must stretch or compress to accommodate the nonnative blend morphology. Chain configurations are different inside dot (circle symbol) and line (square symbol) objects, further highlighting the local chain distortion required to accommodate the morphology. The C chains are evidently more responsive, exhibiting systematic deviations with composition. Reproduced from Ref. [96].

objects; for instance, C chains tend to concentrate to the high-curvature endcaps of line objects. The mixture of chain types affords the opportunity for chains to redistribute spatially to lower overall energy. At the scale of the individual chains, one observes chain distortions to accommodate the nonnative morphological environment [Fig. 4(b)]. In general, C chains are found to be more responsive, in the sense that, in blends, they deviate more strongly from their native conformation (in a cylinder morphology made from pure C material).

MD simulations are also a useful means of probing the time-history of morphology evolution and associated kinetic effects. It was found that blend morphologies can be subject to significant kinetic trapping effects, and thus, the morphologies observed experimentally are due in part to the ordering history. Overall, MD simulations have demonstrated that blending effectively stabilizes defective local motifs, allowing otherwise high-energy morphologies to

form [96,98–100]. This underlying stabilization effect makes blend materials more responsive than pure BCP materials (whose self-assembly is already responsive to local environment). For instance, blends of C and L PS-*b*-PMMA were found to be responsive to supporting surface energy [100], with different morphologies arising depending on substrate wetting conditions (preferential for blocks A, B, or neutral). Of particular note is the wide region—as a function of surface energy and blend composition—where the HPL phase forms. The HPL is metastable in the bulk and experimentally difficult to form in most BCP materials, yet blending evidently enables more robust formation of this morphology. This can be rationalized in terms of defect stabilization, e.g., the perforations can be thought of as high-energy defects that cannot form in a native lamellar BCP but whose internal curvature can be stabilized by preferential localization of C chains.

Beyond athermal blends, AB/AC BCP blends may be used to engineer the assembly of entirely different morphologies with new functionality. Unfavorable B-C interactions ($\chi_{BC} > 0$) tend to increase the likelihood of AB/AC macrophase separation. However, uniformly interspersed microphase separated morphologies may assemble in thin films following a host-guest mechanism within specific ranges of BCP volume fractions, molecular weights, and blend compositions [101–103]. For example, an AB BCP that assembles to a HPL morphology with continuous B domains may serve as a host to self-assembled C spheres of an AC diblock copolymer. Meanwhile, favorable B-C miscibility (e.g., via hydrogen bonding) in AB/AC blends provide a handle for inverting typical curvature-volume fraction relationships. When the lengths of the B and C chains differ, their favorable mixing stretches the shorter of the two chains while compressing the longer one. Since both AC and AB BCPs are pinned to the same domain interfaces, this induces a bending force toward the A layer [104], yielding morphologies like asymmetric lamellae (that is, lamellae with very high A volume fractions) [105], square cylinder arrays [106,107], or cylinders encompassing ∼50% of more of the total system volume [108].

IV. METHODS FOR CHARACTERIZING THIN FILM POLYMER BLEND ASSEMBLY

Blending affords a straightforward way to modify self-assembled morphologies while avoiding new polymer synthesis, with facile control over effective composition. The breadth and precision of compositional control in polymer blends invites researchers to explore a wide range of structure-composition relationships. In bulk samples, the combination of real- and Fourier-space structural characterization in the form of transmission electron microscopy (TEM) and small-angle x-ray scattering (SAXS), respectively, have proven indispensable. These methods naturally complement each other, providing clear interpretation of the morphological structure as well as statistical robustness. Staining (e.g., using osmium tetroxide) is often used in TEM to enhance image contrast. Other ancillary methods may be used to characterize other important properties of the blends; differential scanning calorimetry and Fourier transform infrared spectroscopy have been used to determine thermal properties and the extent of hydrogen bonding, respectively, in the relevant types of blends, for instance [77,82].

In thin films, structural characterization using electron microscopy remains prevalent, though other imaging modalities are made possible by their considerable reduction in one dimension (1D). Scanning electron microscopy (SEM), for example, is often faster and more readily available than TEM. Topographical contrast between domains required for SEM imaging can be achieved by selectively removing [109–111], displacing [112,113], or converting one set of domains [114,115]. Recent years have seen significant interest in liquid [116–118] or vapor phase infiltration synthesis [119–122] of BCP thin films, wherein inorganic material is deposited selectively within one block. The example of vapor phase infiltration, a technique with similarities to atomic layer deposition and often conducted using the same instruments and chemical precursors, is depicted schematically in Fig. 5(a). Whereas ALD is limited by the availability of reaction sites on a solid surface, precursor sorption, diffusion, and reaction within a polymer make deposition throughout a film possible in VPI. Crucially, the polymer must have moieties capable of reacting with the inorganic precursors. Trimethylaluminum, for example, reacts readily with carbonyl and ester groups in PMMA, while phenyl groups in PS are nonreactive. The PMMA is thus selectively infiltrated with alumina. Proper precursor selection and process design ensure uniform but selective deposition of one set of domains throughout a self-assembled polymer film; subsequent removal of the polymeric template yields an inorganic replica of the three-dimensional (3D) morphology of the reactive domains (e.g., PMMA) with high fidelity. Exemplary replicas, characterized by SEM, of the PMMA domain morphology in a vertical hexagonal perforated lamellae phase that emerges from interdiffusion of PS-*b*-PMMA cylinder and lamellae bilayer films are shown in Fig. 5(b).

In addition to electron microscopy, scanning probe microscopies such as atomic force microscopy (AFM) are an accessible alternative in thin films. Though scanning probe techniques do not provide information about the internal 3D domain structure within films, specialized variants like photoinduced force microscopy can yield both topographical and chemical images of self-assembled polymer surfaces [123,124]. In the future, such correlated imaging may provide invaluable details about surface enrichment behavior in polymer blends.

Scattering techniques provide much of the same value in thin films as they do in bulk samples, though methods must often be adapted to account for a different sample geometry. As an example, SAXS may not be well suited for characterizing films only tens of nanometers thick supported on substrates hundreds of micrometers thick if the relevant scattering signal arises from weak electron density contrast from polymer domains. The infiltration synthesis described above presents a viable solution, as it enhances electron density contrast significantly, preserves the substrate-supported domain morphology, and permits electron microscopy on the same samples [99]. Grazing-incidence SAXS (GISAXS) provides another effective option, as the substantial enhancement in scattering volume due to beam projection eliminates the need for further processing to enhance electron density contrast.

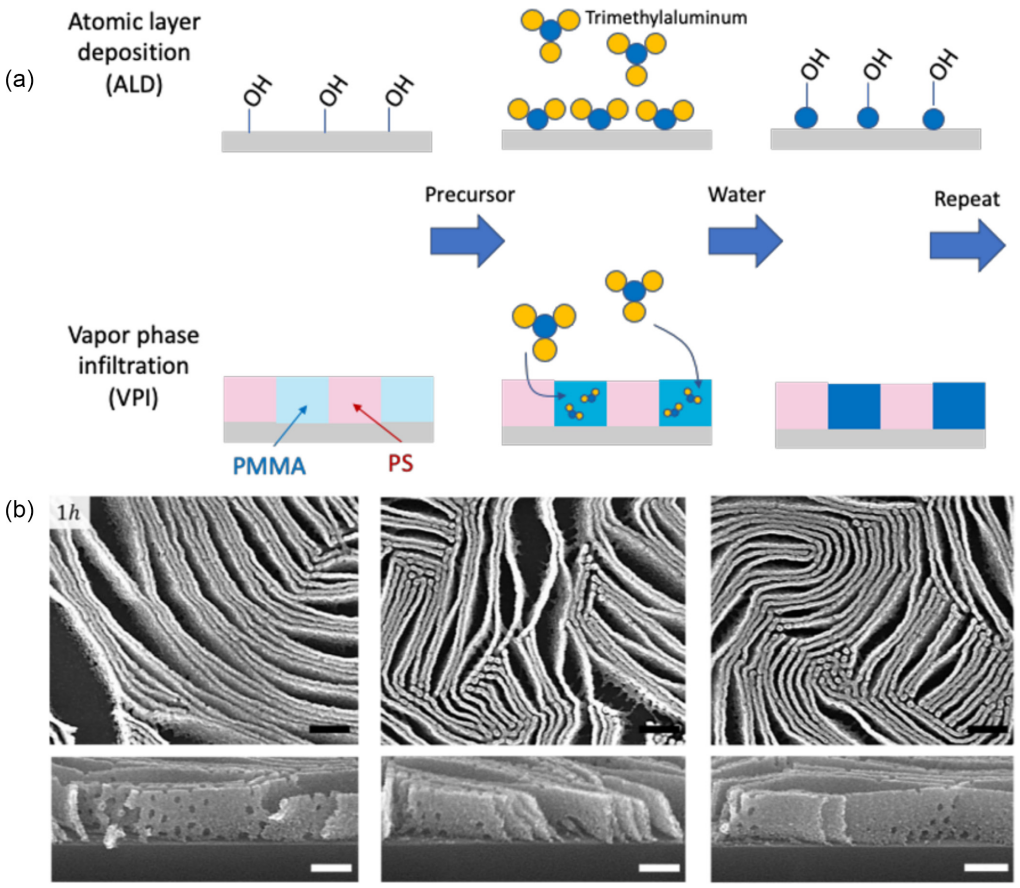

FIG. 5. Enhanced imaging characterization enabled by self-assembled domain replication using vapor phase infiltration (VPI). (a) Schematic of the VPI process. Top row: In atomic layer deposition (ALD) metalorganic precursors attach to an oxidized surface and are fully oxidized (after purging) by subsequent introduction of water. Repeating the process sequence deposits metal oxides with angstrom-level precision. Bottom row: VPI is analogous to ALD and uses the same precursors. However, the precursors are absorbed by the film, diffuse within, and react only with chemical moieties on receptive (generally nonstyrenic) polymers like poly(methyl methacrylate) (PMMA). Repeated exposure deposits metal oxide throughout the receptive domain. Polymer may then be removed by annealing or plasma treatment, generating a mechanically robust, high-fidelity replica of the receptive domain nanostructure. (b) Exemplary top view (top row) and cross-section (bottom row) scanning electron microscope (SEM) images of a vertical hexagonally perforated lamellae (HPL) morphology assembled from a blend of symmetric and asymmetric polystyrene-block-PMMA (PS-*b*-PMMA) block copolymers (BCPs). The PMMA domain morphology is replicated with high fidelity by VPI using aluminum and zinc precursors. All scale bars denote 100 nm. Reproduced from Ref. [98].

Using high-intensity synchrotron x-ray sources, GISAXS can be used to characterize the assembly of polymer blends *in situ* during processing. We utilized this notable feature to understand the self-assembly of ternary blends comprising low molecular weight PS and PMMA ($\sim$3 kg/mol) and symmetric PS-*b*-PMMA BCPs with molecular weights from $\sim$100 to $>$1000 kg/mol during solvent vapor annealing (SVA) [73]. Swelling the films with a near-neutral solvent for PS and PMMA (tetrahydrofuran) screened their interactions, causing the HP to distribute uniformly not just within their domains but throughout the film. This enhanced the effective dilution of the BCP, thus accelerating the self-assembly kinetics while broadening the domain interfaces. Sharper interfaces can be restored by brief thermal annealing that drives resegregation of the HP to alike domains without loss of overall pattern order.

In self-assembling polymer blends, unique and complex morphologies often emerge in narrow regions of the parameter space (e.g., temperature vs volume fraction). Moreover, both practical applications of polymer blends and a deeper understanding of their phase behavior are made possible by capturing detailed trends in structural ordering such as domain spacing, the average length scale of orientational or translational order (correlation length or grain size), and the relative fraction of coexisting morphologies. However, while blending does provide a facile means of achieving broad and precise compositional control, the conventional experimental methods based on serial sample preparation and characterization and offline analysis impede the discovery of morphologies and unusual phase behavior.

Thin films are highly amenable to combinatorial preparation and processing methods that can significantly accelerate investigations into the properties of polymer blend films. Research from the National Institute of Standards and Technology (NIST) demonstrated the compelling case for gradient sample preparation methods, where a property is varied linearly with position across a single dimension. Film thickness can be linearly varied by flow coating (also known as doctor blading) under constant acceleration, as the amount of material deposited is determined by the blade velocity relative to

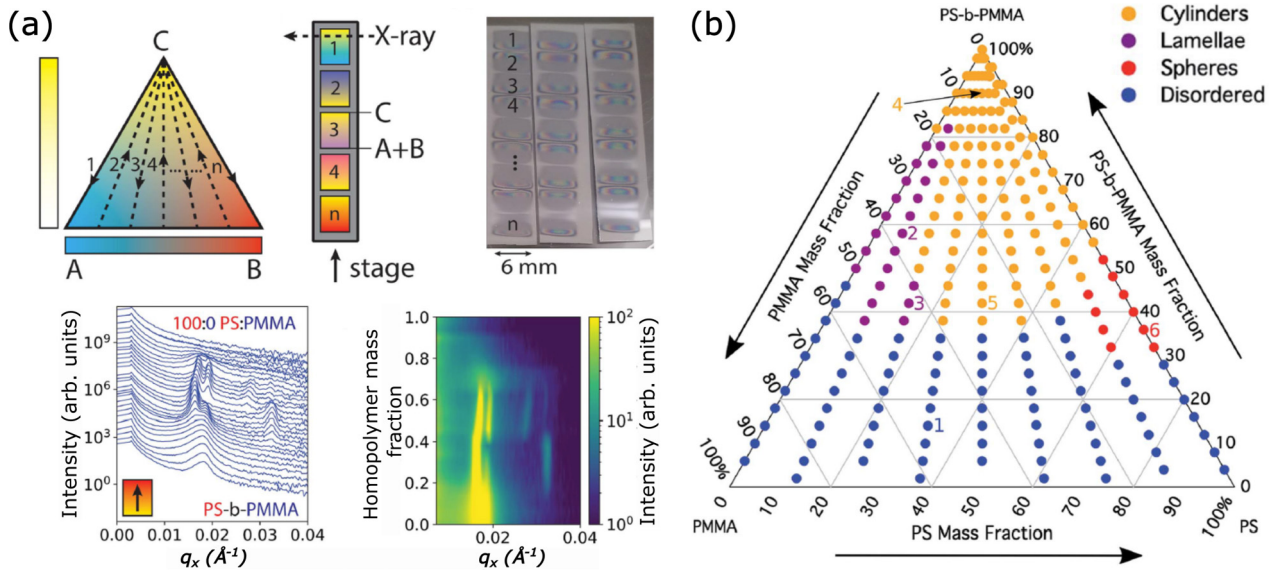

FIG. 6. Combinatorial ternary blend film preparation based on rastered electrospray deposition. (a) Top row: Concept for compiling ternary blend data from multiple composition gradient strips using grazing-incidence small-angle x-ray scattering (GISAXS). Bottom row: Exemplar GISAXS data from one gradient strip showing changes in domain ordering, an order-order transition, and an order-disorder transition with increasing homopolymer (HP) fraction. (b) Full morphology diagram with more than 200 unique measurements for a ternary blend with 67 kg/mol asymmetric polystyrene-block-poly(methyl methacrylate) (PS-*b*-PMMA) and ∼1 kg/mol PS and PMMA Hps. Adapted from Ref. [71].

the substrate [125,126]. The usefulness of this technique was demonstrated in the clear identification of film thicknesses in which horizontal lamellae neat diblock copolymer thin films assemble to form flat surfaces or surfaces textured with islands and/or holes due to the incommensurability between the film thickness and the lamellar domain spacing [127,128].

Substrate surface energy gradients have been prepared by attachment of self-assembled monolayers (SAMs) to substrates followed by gradient ultraviolet (UV) ozonolysis performed using either a gradient neutral density filter or by UV exposure through a slit onto a substrate moving under constant acceleration [129,130]. Alternatively, gradient surface energy can be obtained by cross-diffusive vapor deposition of SAMs under vacuum [131]. Gradient sample annealing has also been demonstrated using a specially designed thermal gradient hot plate [132]. SVA conditions are more challenging to vary controllably due to rapid diffusion; Albert *et al.* [133] overcame this using a microfluidic mixing device placed directly onto a polymer film, which they used to investigate the effect of relative vapor fractions of tetrahydrofuran and heptane on the self-assembly of PS-*block*-PI-*block*-PS (SIS) thin films.

Thin films with linear gradients prepared in the appropriate sequence with a 90 ° rotation between applications yield 2D combinatorial samples. Using this approach, maps of film thickness vs substrate temperature and surface energy have enabled combinatorial investigations of PS dewetting [132] and symmetric PS-*b*-PMMA domain orientation behavior [130]. In general, characterization of combinatorial samples involves low-resolution surveying techniques like optical microscopy and higher-resolution supplemental techniques like AFM or contact angle measurements.

Creating gradient blend composition libraries is comparatively more challenging. Meredith *et al.* [128,134] used multiple syringe pumps to prepare a gradient solution, which was subsequently dispensed along a stripe and then spread as a film by flow coating. While technically challenging, this approach yields a second axis in the flow coating stage motion direction which can be used to vary another parameter such as temperature. This approach was successfully used to ascertain the composition-dependent lower critical solution temperature for a PS/poly(vinyl methy ether) (PS/PVME) blend. The phase behavior is in fact visible to the naked eye in a single optical micrograph based on the optical scattering above and below the cloud point. More recently, linear binary composition gradients have been prepared by flow or slot die coating using fluid dispensed via microfluidic mixing devices [135,136] or by simultaneous spraying from two solutions [137]. We developed an alternative approach based on rastered electrospray deposition to produce thin film ternary blend libraries with bespoke compositional patterns that can be tailored for the application or characterization needs [138]. By designing a series of linear ternary blend gradients that are amenable to high-throughput characterization by synchrotron GISAXS [Fig. 6(a)], this method was used to create a ternary blend morphology diagram for 67 kg/mol C PS-*b*-PMMA blended with 1 kg/mol PS and PMMA HPs with >200 unique measurements across the entire compositional space. These measurements permitted identification of regions with lamellar, cylindrical, spherical, and disordered morphologies [Fig. 6(b)]. The whole process of sample preparation and characterization was completed within a single day, with most of the time (>12 h) allotted to thermal annealing in a vacuum oven. The excellent data granularity revealed the positions of order-disorder and order-order transitions with as high as ∼4% resolution as well as systematic trends in domain spacing and grain size [71]. This same approach was also used to prepare and characterize blends of 75 kg/mol

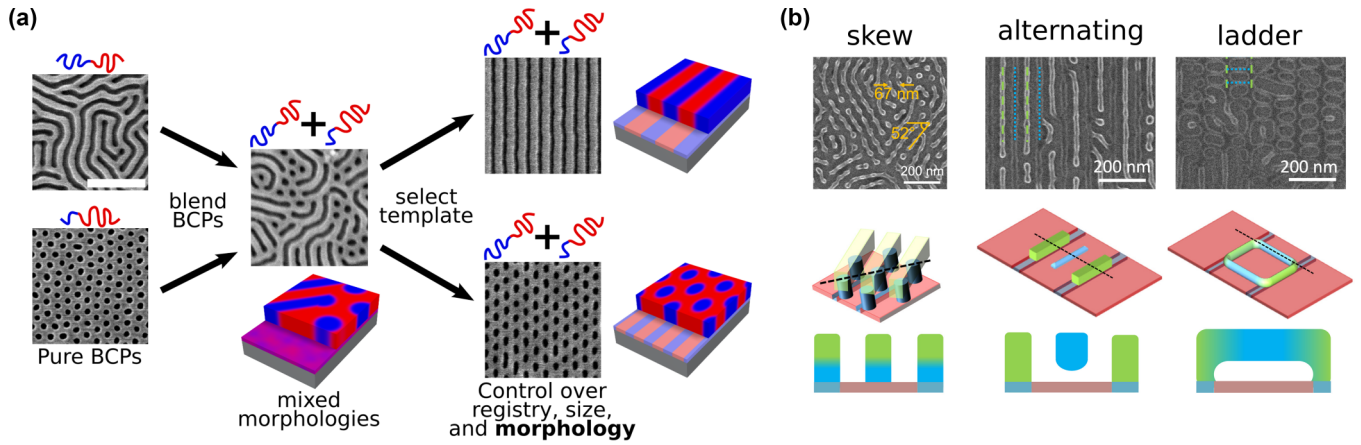

FIG. 7. (a) Blends of block copolymers (BCPs) can form coexistence phases in thin films. An underlying chemical grating can select which morphology locally forms since the grating line width and spacing impose differing energy penalties on the different structures. Reproduced from Ref. [147]. (b) Exploring a broader range of chemical gratings led to the discovery of three-dimensional (3D) morphologies, including skew (lamellar lines bridging underlying cylinders), alternating (lamellarlike and cylinderlike lines), and ladder (lamellarlike rails connected by cylinderlike rungs). In the diagrams, green is used to denote lamellarlike structures and blue to denote cylinderlike. However, both underlying BCP chain types contribute to structure formation throughout the morphology. Adapted from Ref. [99].

symmetric PS-*b*-PMMA with gradient volume fractions of PS and PMMA HPs in a 1:1 ratio, where the film thickness and HP molecular weight were varied. In combination with gradient thickness flow coating and MD simulations, the rich data revealed how the interplay between film thickness and HP fraction due to HP surface enrichment alters the domain orientation and even measured periodicity [72].

The inherent responsiveness of blends to external stimuli via phenomena like chain redistribution and surface enrichment suggests that blends subjected to constraints may assemble into a host of nonnative nanoscale morphologies. Accounting for the effects of not just blend composition but also directing forces, complex boundary conditions, and intricate ordering histories, however, implies an enormous parameter space that even advanced combinatorial approaches are ill-equipped to explore. To address this, researchers have begun taking advantage of artificial intelligence and machine-learning (AI/ML) methods to accelerate experimental studies and thus material discovery. Autonomous experimentation (AE) seeks to automate measurement loops [139–141], using AI/ML decision-making agents to select high-value experiments based on the growing dataset. Going beyond mere preprogrammed automation, these methods actively model the problem being explored, allowing them to select valuable experiments to perform on each iteration of the loop. Of particular relevance to the study of self-assembling thin films is the recent demonstration of autonomous x-ray scattering at synchrotron beamlines [142–146]. This involves automating the synchrotron measurement and x-ray scattering data analysis. A Gaussian process method is used to model the accumulating data, generating a surrogate model (prediction for signals of interest as a function of physical parameters) and a corresponding uncertainty. The ML objective can be tailored to experimental needs. In a generic AE where the goal is to efficiently search a parameter space, one can select high-uncertainty regions in the space for measurement on each loop. This efficiently maximizes the rate of knowledge gain, but these methods can also be tailored to focus attention on features of interest or to search for novelty. Overall, AE methods are poised to accelerate material discovery and have already been successfully applied to discovery of BCP morphologies (see below).

V. COMPLEX STRUCTURES

Blending of different BCP chains affords the opportunity to stabilize high-energy local motifs, which enables the formation of morphologies that would otherwise not form. Blending can be used to stabilize equilibrium or metastable morphologies, such as tuning the domain spacing and orientation of an equilibrium morphology [72], stabilizing the elusive HPL morphology [100], or generating coexistence phases of familiar motifs [92]. Blending can also be exploited to generate more complex structures, by combining it with other driving forces or priming the system in a contrived state. Indeed, nonnative structures more naturally arise when the BCP ordering is subject to constraints, such as thin film confinement or prescribed ordering history.

Blends of C and L BCPs were applied to chemically patterned substrates to investigate the role of this strong directing field [147]. It was found that chemical line patterns could select between the dot and line morphologies [Fig. 7(a)]. That is, the morphology that appeared depended on the width and/or spacing of the underlying chemical stripes. It is natural to expect that the line morphology would be robustly enforced by chemical stripes matching the spacing and linewidth of the blend BCP. It is less obvious why nonmatching chemical stripe widths or spacings instead cause the film to form a hexagonal array of dots. Simple energetic arguments can be constructed by considering two effects: the distortion of the unit cell to align with the given chemical pattern (which introduces energy penalties due to distortion of the underlying chains) and the chemical mismatch between the morphology and the pattern (incurring enthalpic penalties). This energy

model rationalizes the formation of dot patterns when the chemical pattern is sufficiently mismatched. Qualitatively, one can say that the dot pattern suffers greater chemical mismatch (in terms of favorable overlap of the BCP pattern and the substrate pattern), but the dot pattern is more tolerant to unit-cell distortion. This is because, in the line pattern, all the BCP chains must distort to accommodate length-scale mismatch (since all chains are aligned orthogonal to the grating repeat direction), whereas for the dot pattern, many of the chains are at other angles and remain relatively unperturbed by unit cell stretching. Overall, these results demonstrate the precisely responsive nature of blends, where directing forces can be used to select among competing structural motifs. Indeed, it was shown that using substrate chemical patterns that vary spatially allows one to prescriptively define morphologies spatially. This enabled the defined formation of regions of line patterns and dot patterns and even the formation of, e.g., a single isolated column of dots in a field of lines.

The responsiveness of BCP blends to chemical templates suggests that more exotic thin film morphologies could exist in the broad parameter space defined by blend formulations and chemical pattern designs. To explore this enormous space, AE methods were applied. Electron-beam lithography was used to generate a dense array of chemical patterns, varying grating pitch (Λ) and stripe width (via e-beam dose) [99]. A blend of C and L material was cast on this substrate and thermally annealed; this single sample acts as a combinatorial library of every possible ordering condition (for the given blend ratio and film thickness). An AE measurement loop at a synchrotron x-ray scattering beamline was then used to explore this space, with the decision-making algorithm designed to reconstruct models for scattering at different azimuthal angles (which could correspond to different ordering motifs). In this rapid AE search, researchers immediately observed the previously identified morphologies (well-ordered dot and line patterns near $\Lambda \approx L_0$). However, several unanticipated morphologies were also discovered [Fig. 7(b)]. In the vicinity of $\Lambda \approx 2L_0$, the blend formed alternating stripes of lamellae lines (reaching to the substrate) and cylinder lines (separated from the substrate by a wetting layer). For slightly thinner chemical stripes, a ladder morphology instead formed, with lamellaelike rails cross-connected by cylinderlike rungs. In the intermediate regime ($L_0 < \Lambda < 2L_0$), the thin film forms a skew morphology, with substrate attached cylinder legs connected to top-surface lamellarlike lines that are not aligned to the grating. In this regime, the morphology cannot be commensurate if orientationally aligned with the grating, and so it instead reconstructs with a skew angle and structural partitioning in the film thickness direction. In fact, these three morphologies all exhibit 3D ordering as part of the attempt of the blend to reconcile structure formation with the underlying chemical pattern. This exploration highlights the much larger diversity of possible self-assembled morphologies compared with the conventional equilibrium phase diagram of pure BCP materials. It also confirms the intuition that strong directing fields can be used to select among competing states, thereby diversifying the range of structures that BCPs form.

Explicit control of structure formation in the film thickness direction can be applied by layering BCP materials. In earlier work, BCPs were iteratively stacked in a prescriptive manner. Each layer can be converted into an (immobilized) inorganic replica, allowing additional layers to be placed on top without disrupting the underlayer(s). For instance, photothermal annealing was used to shear-align BCPs [148–150], followed by infiltration synthesis to convert into metal or metal oxide replicas. Application of subsequent layers enabled the formation of arbitrary 2D lattice symmetries by controlling the angle between shear steps [151]. In another study, BCP phases were immobilized to allow additional layers to order in response to the underlayer (templating off of the subtle height variation afforded by the BCP morphology). In this way, 3D structures arose naturally owing to the registered assembly of the second layer [152]. These examples demonstrate controlled formation of 3D structures, but they do not fully leverage the responsiveness of BCP materials since underlying layers are structurally frozen. An alternative strategy is to layer BCPs without immobilization. Bilayers of different BCP materials, once annealed, should undergo nontrivial self-assembly since the two layers will tend to interdiffuse on the same time scale as intrinsic phase separation and self-assembly in each layer. This kind of layering of different BCP materials can be thought of as a structured blend. In more recent work, these configurations were studied [98]. Annealing of these stacked BCP systems gives rise to a host of morphologies (Fig. 8), many of which are transient as they occur only as intermediate states as the two layers mix. Even after long annealing, however, the structures that are present may be nontrivial and may not match what one would obtain from annealing a single-layer blend of the same total thickness (i.e., initial condition with homogenous chain distribution). This can occur due to kinetic trapping (pathway-dependent ordering) or energetic stabilization of nonuniform chain mixing.

More specifically, researchers identified four design principles that explain the formation of nonnative structures for annealing of BCP bilayers. First, at early annealing times, local phase separation occurs before complete mixing between the layers has completed. As a result, early morphologies often bear the hallmark of the intrinsic morphologies. For instance, layering C on top of L material gives rise to a parapet structure where lamellarlike walls near the substrate are decorated with cylinderlike caps near the free surface (though this structure does not persist with further annealing). Second, the mixture of chain types can stabilize structure defects (e.g., perforations, domain antialignment, or coexistence phases) since the underlying chains can reorganize during layer mixing. This enables the formation of vertical HPL morphology, where C chains concentrate around the perforations and stabilize these high-curvature regions. While the greater configurational freedom afforded by blending can stabilize exotic morphologies, it can also lead to more defective structures (such as the formation of patchwork morphologies characterized by randomly interconnected struts). Third, one of the two underlying chain types might preferentially segregate to interfaces, stabilizing a nonuniform structure in the film normal direction. The C chains tend to segregate at interfaces (for entropic reasons associated with their shorter minority-block chain ends). This gives rise to the stabilization of an aqueduct morphology, with substrate-attached cylinderlike columns supporting lamellarlike walls at the film surface.

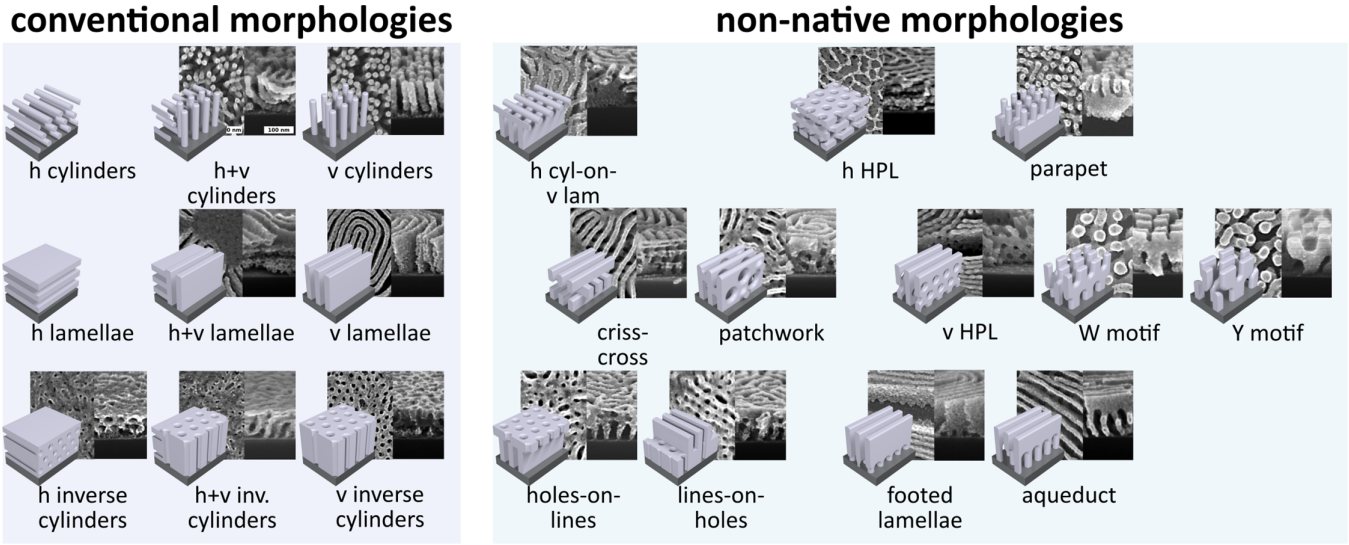

FIG. 8. A diverse library of nanostructures can arise when layering simple block copolymer materials (cylinder, inverse-cylinder, and lamellae-forming). Both conventional and nonnative morphologies can appear. The latter arise due to the configurational freedom afforded by the mixture of chain types. Adapted from Ref. [98].

This morphology is stable, even for long annealing times. Modifying the molecular weight of the two BCPs can suppress or exacerbate this effect. For instance, W and Y motifs are generated in cases where the C chains even more strongly segregate to both interfaces. Fourth, it was observed that there were substantial energy barriers to interconversion between states, leading to the kinetic trapped morphologies (such as coexistence of vertical and horizontal states). This highlights how self-assembly is pathway dependent (particularly in BCP thin films where ordering can be frustrated) and correspondingly highlights a pathway-priming strategy for controlled structure formation. That is, a particular morphology can be selected by engineering the correct starting configuration (layering of BCP materials) and terminating annealing at the appropriate time. In effect, one can select among pathways in the complex, high-dimensional ordering landscape to create a desired structure.

VI. DESIGN RULES

Decades of research have progressively yielded an evermore detailed description of the landscape for polymer blend assembly, which may eventually enable prescriptive formation of complex nanostructures through judicious control of polymer architecture, blend composition, processing history, boundary conditions, and directing fields. Here, we outline design rules and guiding principles for directing the assembly of polymer blend thin films that may be derived from several general considerations: enthalpic vs architectural disparity of the blended components, the constraints imposed by dimensional confinement, and pathway-dependent morphological metastability.

The first consideration is interactions between the blended components which apply in both thin films and the bulk. As noted previously, enthalpic interactions play a central role, where favorable mixing interactions compatibilize components, while unfavorable interactions lead to complete macrophase separation except under a narrow set of conditions. On the other hand, the large body of research on athermal blends has helped isolate the effects of blending components with disparate macromolecular architectures, which alters the conformational entropy of the system. Much of the intriguing assembly behavior that has been observed in polymer blends can be loosely classified based on the strength of component interactions along axes of enthalpic disparity and architectural disparity (Fig. 9). At one extreme of the enthalpic disparity axis, all component interactions are strongly unfavorable, leading to macrophase separation; component interactions at the other extreme are all strongly favorable, and the resulting compatibilization promotes a high degree of mixing. Self-assembly in blends must necessarily occur within these limits.

Architectural disparity is comparatively more subtle. At one extreme are neat BCP melts, which can be considered degenerate blends with minimal architecture variation (e.g., a linear AB BCP blended with the same AB BCP). Athermal blends of a symmetric linear diblock copolymer with a chemically alike asymmetric diblock copolymer represent a step toward increased architectural disparity. In many cases, the blends form a single morphology identical to that of one of the components (e.g., lamellae or cylinders). However, the ability of the chains to redistribute to maximize conformational entropy while pinning the chemical junction to the domain interface can promote the assembly of a separate bicontinuous phase or coexisting phases. Defect stabilization can even produce entirely new morphologies, such as the ladder shown in Fig. 7. BCP/HP blends represent a further increase in architectural disparity by eliminating one block entirely. Lacking a chemical junction, the HP is less restricted in the ways it can distribute throughout its domain and may therefore occupy interstices or localize to domain centers. An even higher degree of architectural disparity may be accessed by using blends comprising triblock copolymers, BCPs possessing blocks with higher conformational asymmetry, or

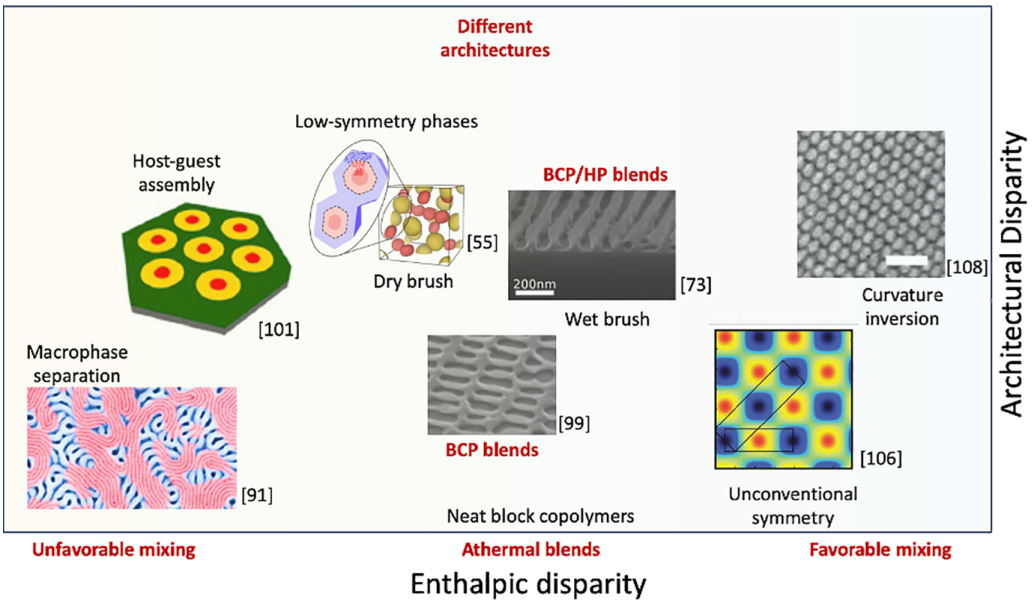

FIG. 9. Landscape for interactions between blended polymers, which can be loosely categorized along axes of enthalpic and architectural disparity. Unfavorable mixing interactions are parameterized by positive χ values, while favorable mixing interactions are parameterized by negative ones. Athermal blends feature chemically identical components. However, the differences in polymer architecture change the entropic constraints of the system. AB block copolymer (BCP) blends with different volume fractions and BCP/homopolymer (HP) blends can either alleviate or cause packing frustration, or stabilize localized defects, both of which can alter the assembled morphologies. Blends of BCPs with different architectures increase the architectural disparity even further. Unfavorable mixing generally leads to macrophase separation, though stable morphologies with host-guest interactions can be obtained with some architectural disparity. Favorable mixing interactions, on the other hand, aid compatibilization. Enthalpically driven chain stretching or compression modifies the curvature relationships from those encountered in athermal blends. Portions adapted from Refs. [55,73,91,99,101,108]. Copyrights 2015, 2020, and 2021, American Chemical Society. Portion adapted from Ref. [106]. Reprinted with permission from AAAS.

polymers blends featuring star, bottle brush, or other differing nonlinear architectures.

Though the effects of architectural disparity are most easily recognized in athermal blends, unique morphologies may be assembled through intelligent combinations of enthalpic and architectural disparity. As noted earlier, AB/AC BCP blends with favorable B-C mixing exhibit a bending force toward the A domain when there is a difference in the B and C block volumes. This can engender new symmetries (e.g., square lattices) or invert the normal domain curvature. On the other hand, well-ordered host-guest self-assembly is made possible for unfavorable B-C mixing only when the architectural disparity is chosen carefully such that C guest domains (within the BC BCP) can naturally position in a low-energy state among host A domains (within the AB BCP).

The second consideration is the profound implications of dimensional confinement on blend self-assembly. Though the effects may be more pronounced in 2D (e.g., cylindrical confinement) or 3D (e.g., spherical confinement), we focus on 1D (i.e., thin film) confinement based on its technological importance for nanopatterning and to more easily highlight the interrelated ways in which confinement can induce morphological change. In very thin films, the confluence of block surface energies and commensurability between the film thickness and domain spacing dictates the orientation of domains with respect to the film surface. If one block has a lower energy at either the substrate or air interface, domains will orient horizontally to permit wetting of that block at the appropriate interface. In diblock copolymers, for instance, lowest-energy states in diblock copolymers are obtained when the film thickness is equal to an integer (n) multiple of the domain period (L_0) if one block preferentially wets both surfaces or when the film thickness is equal to $(n + {}^1/_2)L_0$ if each surface is wet preferentially by the other block. Film thicknesses incommensurate with these quantized values impose an entropic penalty due to chain stretching or compression required to maintain a horizontal domain orientation. Depending on the degree of wetting asymmetry by the blocks, these penalties can promote vertical domain orientation, induce polymer reorganization to form microscale island or hole structures that maintain an overall commensurate film thickness, or even drive the assembly of morphologies not available in the bulk [3,29]. By stabilizing defects or redistributing chains in ways that are impossible for neat BCPs, blends can potentially alter how film thickness commensurability affects domain orientation or morphology.

Even when surfaces have been engineered to achieve balanced interfacial energies among the blocks, blending can influence the morphology in thin films through preferential component enrichment at film surfaces. As discussed earlier, for instance, entropic attraction for shorter polymers to film interfaces drives surface enrichment by HPs in wet brush BCP/HP blends, thereby creating a HP wetting layer(s). Interplay between wetting layer formation and incommensurability effects results in thickness-dependent domain reorientation. It is also well recognized that preferential adsorption of blocks at BCP film interfaces can change important properties like the order-disorder transition [153–155] and domain interfacial

width [156]. Blending components with different enthalpic preferences for surfaces or high architectural disparity will modify the surface adsorption behavior and thereby alter assembly boundary conditions.

At a higher level of abstraction, confinement also affects the symmetries that may be observed. A hard surface breaks the translational symmetry of a 3D lattice, enforcing 2D packing motifs in proximity to the surface. This explains the proclivity for hexagonal sphere packing and the HPL phase in very thin films. As noted earlier, HP has been shown to extend the thickness of surface-induced packing in BCP/HP binary blends. The role of surface enrichment in this context remains unclear, however. Moreover, blends with higher architectural disparity may realize different 2D packing motifs, which evolve through other possible complex morphologies with increasing film thickness.

The third consideration is the possible effects of kinetic trapping and pathway-dependent assembly behavior. In polymer self-assembly, the pathway to the ultimate structure is sensitive to the details of the processing steps utilized, such as casting method, annealing time and temperature (or solvent), and applied fields. This sensitivity facilitates *pathway engineering*, in which processes are designed to realize desirable structures that are inaccessible with a single step process. The pathway-priming approach described above is a notable case [98]. In another striking example, shearing a BCP film rapidly—even faster than the time in which phase separation can occur—instills latent alignment along the shear direction that guides assembly toward a globally aligned morphology during subsequent isotropic thermal annealing, which normally produces a poly-grain morphology [157,158]. Pathway engineering is a powerful means to direct self-assembly, but it is challenging to explore various material combinations within a single neat BCP system; blending introduces opportunities to tune material properties (e.g., domain stiffness, free volume, relaxation times) by which to efficiently explore and modify pathways to metastable morphologies.

Alternatively, the difference in responsivity of various components in a blend makes it possible to realize metastable morphologies through pathway engineering that are inaccessible using neat BCPs. Returning to an earlier example, swelling a ternary blend of PS-*b*-PMMA with superwet brush PS and PMMA HPs by vapors of tetrahydrofuran (THF), a weakly selective solvent that screens polymer interactions, results in uniform distribution of the HP throughout the film, not just within domains. This enhances the effective dilution, accelerating ordering kinetics substantially such that long-range pattern order can be achieved even with an UHMW BCP. After a rapid quench, the uniformly distributed HP broadens that domain interfaces, resulting in extremely rough patterns. This can be rectified by a very brief thermal anneal ($\sim$30 s), which drives HP resegregation without significant changes in the overall pattern order, yielding a highly ordered pattern with smooth features that can be readily transferred to other materials. Longer thermal annealing, however, destroys the pattern as HP migrates to topological defect sites (i.e., pattern dislocations and disclinations) [73]. Thus, pathway engineering in these blends produces a valuable metastable structure much more rapidly than can be achieved using a neat BCP.

VII. PERSPECTIVES

Looking to the future, we see a rich set of possible research directions. There is now ample evidence that blending can enable the emergence of complex nanostructures in a controlled way, using rather simple and readily available starting materials as inputs. Blending is complementary to polymer synthesis, in the sense that the synthesis of new chain architectures correspondingly opens new parts of the overall blending parameter space. It also appears that the range of structures that form are more diverse when blends are subjected to constraints (confinement, directing fields, and ordering histories) that drive them further from the bulk equilibrium regime. This suggests that the full landscape of BCP blends has even more interesting and exotic structures waiting to be discovered. Thus, an obvious future research direction is to more exhaustively explore the possibilities afforded by blending BCP materials. More exotic morphologies should be possible once one admits multicomponent blends (of $\geqslant$3 self-assembling materials) and more exotic chain architectures (such as bottlebrush copolymers). This search is challenging, however, owing to the enormity of a parameter space defined by blend composition (including mass fraction and chain characteristics) convolved with processing history—both conventional processing (such as thermal annealing) as well as blend-specific aspects (such as priming a blend in a nontrivial spatialized manner). To efficiently explore this space will require isolating and elucidating the relevant effects.

One useful insight may be to consider HP, BCP, and blend materials as merely special cases of the overall space defined by the intersection of chain architecture with blend composition. For instance, a pure diblock BCP melt is in fact a blend with a distribution of molecular weights, i.e., a 2D distribution over the lengths of the two blocks. In this sense, much could be learned by studying BCP morphology evolution as a function of these distributions, which can be artificially generated by mixing different pure materials in different ratios. Indeed, the robust self-assembly of pure BCP materials may arise in part from the combination of different chain lengths, which are able to locally redistribute to stabilize the morphology. Along these lines, it would be valuable to consider different BCP chain architectures as being variants of one another to gain more insights into the effects of architectural disparity. Similarly, blending conventional diblock copolymers with tapered, block-random, and other sequence-defined copolymers can be used to clarify the effects of varying enthalpic disparity on self-assembly. Recent advances in precision synthesis are expected to be invaluable for realizing an ample supply of bespoke components with prescribed chain sequences and architectures [159–164]. Combining the results of such studies will elucidate the general underlying rules that dictate which morphology is lowest energy. Indeed, the field has already identified many salient factors, including the usual BCP design rules (minimize interfacial area, interfacial curvature dictated by conformational and architectural asymmetry, etc.) and the emerging blend design rules (defect stabilization, pathway dependency, etc.).

Overall, blending of self-assembling polymers is emerging as a powerful strategy for improving control of the self-assembly process, through phenomena like accelerated

ordering kinetics and the stabilization of noncanonical structural motifs. Thus, it can be viewed as another tool in the BCP toolbox, which can be deployed where appropriate to solve challenges to material ordering.

[1] F. S. Bates and G. H. Fredrickson, Block copolymers—Designer soft materials, Phys. Today **52**(2), 32 (1999).

[2] F. S. Bates and G. H. Fredrickson, Block copolymer thermodynamics: Theory and experiment, Annu. Rev. Phys. Chem. **41**, 525 (1990).

[3] J. N. L. Albert and T. H. Epps, Self-assembly of block copolymer thin films, Mater. Today **13**, 24 (2010).

[4] S. O. Kim, H. H. Solak, M. P. Stoykovich, N. J. Ferrier, J. J. De Pablo, and P. F. Nealey, Epitaxial self-assembly of block copolymers on lithographically defined nanopatterned substrates, Nature (London) **424**, 411 (2003).

[5] M. P. Stoykovich, M. Müller, S. O. Kim, H. H. Solak, E. W. Edwards, J. J. de Pablo, and P. F. Nealey, Directed assembly of block copolymer blends into nonregular device-oriented structures, Science **308**, 1442 (2005).

[6] S. Park, D. H. Lee, J. Xu, B. Kim, S. W. Hong, U. Jeong, T. Xu, and T. P. Russell, Macroscopic 10-terabit–per–square-inch arrays from block copolymers with lateral order, Science **323**, 1030 (2009).

[7] R. Ruiz, H. Kang, F. A. Detcheverry, E. Dobisz, D. S. Kercher, T. R. Albrecht, J. J. de Pablo, and P. F. Nealey, Density multiplication and improved lithography by directed block copolymer assembly, Science **321**, 936 (2008).

[8] J. Y. Cheng, C. T. Rettner, D. P. Sanders, H.-C. Kim, and W. D. Hinsberg, Dense self-assembly on sparse chemical patterns: Rectifying and multiplying lithographic patterns using block copolymers, Adv. Mater. **20**, 3155 (2008).

[9] H.-C. Kim, S.-M. Park, and W. D. Hinsberg, Block copolymer based nanostructures: Materials, processes, and applications to electronics, Chem. Rev. **110**, 146 (2010).

[10] I. Bita, J. K. W. Yang, Y. S. Jung, C. A. Ross, E. L. Thomas, and K. K. Berggren, Graphoepitaxy of self-assembled block copolymers on two-dimensional periodic patterned templates, Science **321**, 939 (2008).

[11] H. Tsai, J. W. Pitera, H. Miyazoe, S. Bangsaruntip, S. U. Engelmann, C.-C. Liu, J. Y. Cheng, J. J. Bucchignano, D. P. Klaus, E. A. Joseph *et al.*, Two-dimensional pattern formation using grapho-epitaxy of PS-*b*-PMMA block copolymers for advanced FinFET device and circuit fabrication, ACS Nano **8**, 5227 (2014).

[12] G. S. Doerk, J. Y. Cheng, G. Singh, C. T. Rettner, J. W. Pitera, S. Balakrishnan, N. Arellano, and D. P. Sanders, Enabling complex nanoscale pattern customization using directed self-assembly, Nat. Commun. **5**, 5805 (2014).

[13] V. Abetz, Isoporous block copolymer membranes, Macromol. Rapid Commun. **36**, 10 (2015).

[14] S. Greil, A. Rahman, M. Liu, and C. T. Black, Gas transport selectivity of ultrathin, nanoporous, inorganic membranes made from block copolymer templates, Chem. Mater. **29**, 9572 (2017).

[15] S. Y. Yang, I. Ryu, H. Y. Kim, J. K. Kim, S. K. Jang, and T. P. Russell, Nanoporous membranes with ultrahigh selectivity and flux for the filtration of viruses, Adv. Mater. **18**, 709 (2006).

[16] C. Li, L. Wen, X. Sui, Y. Cheng, L. Gao, and L. Jiang, Large-scale, robust mushroom-shaped nanochannel array membrane for ultrahigh osmotic energy conversion, Sci. Adv. **7**, eabg2183 (2021).

[17] N. Hampu, J. R. Werber, W. Y. Chan, E. C. Feinberg, and M. A. Hillmyer, Next-generation ultrafiltration membranes enabled by block polymers, ACS Nano **14**, 16446 (2020).

[18] A. Rahman, A. Ashraf, H. Xin, X. Tong, P. Sutter, M. D. Eisaman, and C. T. Black, Sub-50-Nm self-assembled nanotextures for enhanced broadband antireflection in silicon solar cells, Nat. Commun. **6**, 5963 (2015).

[19] A. C. Liapis, A. Rahman, and C. T. Black, Self-assembled nanotextures impart broadband transparency to glass windows and solar cell encapsulants, Appl. Phys. Lett. **111**, 183901 (2017).

[20] P. Mokarian-Tabari, R. Senthamaraikannan, C. Glynn, T. W. Collins, C. Cummins, D. Nugent, C. O'Dwyer, and M. A. Morris, Large block copolymer self-assembly for fabrication of subwavelength nanostructures for applications in optics, Nano Lett. **17**, 2973 (2017).

[21] Z. Diao, M. Kraus, R. Brunner, J.-H. Dirks, and J. P. Spatz, Nanostructured stealth surfaces for visible and near-infrared light, Nano Lett. **16**, 6610 (2016).

[22] J. Y. Kim, H. Kim, B. H. Kim, T. Chang, J. Lim, H. M. Jin, J. H. Mun, Y. J. Choi, K. Chung, J. Shin *et al.*, Highly tunable refractive index visible-light metasurface from block copolymer self-assembly, Nat. Commun. **7**, 12911 (2016).

[23] A. A. Kulkarni and G. Doerk, Thin film block copolymer self-assembly for nanophotonics, Nanotechnology **33**, 292001 (2022).

[24] A. A. Kulkarni and G. S. Doerk, Hierarchical, self-assembled metasurfaces via exposure-controlled reflow of block copolymer-derived nanopatterns, ACS Appl. Mater. Interfaces **14**, 27466 (2022).

[25] A. Checco, A. Rahman, and C. T. Black, Robust superhydrophobicity in large-area nanostructured surfaces defined by block-copolymer self assembly, Adv. Mater. **26**, 886 (2014).

[26] T. Mouterde, G. Lehoucq, S. Xavier, A. Checco, C. T. Black, A. Rahman, T. Midavaine, C. Clanet, and D. Quéré, Antifogging abilities of model nanotextures, Nat. Mater. **16**, 658 (2017).

[27] A. Al Hossain, M. Yang, A. Checco, G. Doerk, and C. E. Colosqui, Large-area nanostructured surfaces with tunable zeta potentials, Appl. Mater. Today **19**, 100553 (2020).

[28] A. A. Hossain, A. Dick, G. Doerk, and C. E. Colosqui, Toward controlling wetting hysteresis with nanostructured surfaces derived from block copolymer self-assembly, Nanotechnology **33**, 455302 (2022).

[29] G. S. Doerk and K. G. Yager, Beyond native block copolymer morphologies, Mol. Syst. Des. Eng. **2**, 518 (2017).

[30] R. Liang, Y. Xue, X. Fu, A. N. Le, Q. Song, Y. Qiang, Q. Xie, R. Dong, Z. Sun, C. O. Osuji *et al.*, Hierarchically engineered nanostructures from compositionally anisotropic molecular building blocks, Nat. Mater. **21**, 1434 (2022).

[31] Z. Sun, R. Liu, T. Su, H. Huang, K. Kawamoto, R. Liang, B. Liu, M. Zhong, A. Alexander-Katz, C. A. Ross *et al.*, Emergence of layered nanoscale mesh networks through intrinsic

molecular confinement self-assembly, Nat. Nanotechnol. **18**, 273 (2023).

[32] P. C. Painter and M. M. Coleman, *Fundamentals of Polymer Science: An Introductory Text* (CRC Press, Boca Raton, 1997).

[33] M. Banaszak and M. D. Whitmore, Mean field theory of the lamellar structure of block copolymer/homopolymer blends in the weak segregation regime, Macromolecules **25**, 2757 (1992).

[34] D. Broseta and G. H. Fredrickson, Phase equilibria in copolymer/homopolymer ternary blends: Molecular weight effects, J. Chem. Phys. **93**, 2927 (1990).

[35] K. H. Dai, E. J. Kramer, and K. R. Shull, Interfacial segregation in two-phase polymer blends with diblock copolymer additives: The effect of homopolymer molecular weight, Macromolecules **25**, 220 (1992).

[36] T. Hashimoto, H. Tanaka, and H. Hasegawa, Ordered structure in mixtures of a block copolymer and homopolymers. 2. effects of molecular weights of homopolymers, Macromolecules **23**, 4378 (1990).

[37] T. Hashimoto, S. Koizumi, and H. Hasegewa, Interfaces in block copolymer/homopolymer mixtures forming dry brushes, Physica B **213–214**, 676 (1995).

[38] P. K. Janert and M. Schick, Phase behavior of ternary homopolymer/diblock blends: Influence of relative chain lengths, Macromolecules **30**, 137 (1997).

[39] S. Koizumi, H. Hasegawa, and T. Hashimoto, Spatial distribution of homopolymers in block copolymer microdomains as observed by a combined SANS and SAXS method, Macromolecules **27**, 7893 (1994).

[40] M. W. Matsen, Phase behavior of block copolymer/homopolymer blends, Macromolecules **28**, 5765 (1995).

[41] M. W. Matsen, Stabilizing new morphologies by blending homopolymer with block copolymer, Phys. Rev. Lett. **74**, 4225 (1995).

[42] N. Torikai, N. Takabayashi, I. Noda, S. Koizumi, Y. Morii, and Y. Matsushita, Lamellar domain spacings of diblock copolymer/homopolymer blends and conformations of block chains in their microdomains, Macromolecules **30**, 5698 (1997).

[43] X. Quan, I. Gancarz, J. T. Koberstein, and G. D. Wignall, Effect of homopolymer molecular weight on the morphology of block copolymer/homopolymer blends, Macromolecules **20**, 1431 (1987).

[44] K. R. Shull and K. I. Winey, Homopolymer distributions in lamellar copolymer/homopolymer blends, Macromolecules **25**, 2637 (1992).

[45] H. Tanaka, H. Hasegawa, and T. Hashimoto, Ordered structure in mixtures of a block copolymer and homopolymers. 1. Solubilization of low molecular weight homopolymers, Macromolecules **24**, 240 (1991).

[46] K. I. Winey, E. L. Thomas, and L. J. Fetters, Ordered morphologies in binary blends of diblock copolymer and homopolymer and characterization of their intermaterial dividing surfaces, J. Chem. Phys. **95**, 9367 (1991).

[47] K. I. Winey, E. L. Thomas, and L. J. Fetters, Swelling of lamellar diblock copolymer by homopolymer: Influences of homopolymer concentration and molecular weight, Macromolecules **24**, 6182 (1991).

[48] K. I. Winey, E. L. Thomas, and L. J. Fetters, Isothermal morphology diagrams for binary blends of diblock copolymer and homopolymer, Macromolecules **25**, 2645 (1992).

[49] G. Liu, M. P. Stoykovich, S. Ji, K. O. Stuen, G. S. W. Craig, and P. F. Nealey, Phase behavior and dimensional scaling of symmetric block copolymer-homopolymer ternary blends in thin films, Macromolecules **42**, 3063 (2009).

[50] A. D. Goodson, G. Liu, M. S. Rick, A. W. Raymond, M. F. Uddin, H. S. Ashbaugh, and J. N. L. Albert, Nanostructure stability and swelling of ternary block copolymer/homopolymer blends: A direct comparison between dissipative particle dynamics and experiment, J. Polym. Sci. B **57**, 794 (2019).

[51] K. O. Stuen, C. S. Thomas, G. Liu, N. Ferrier, and P. F. Nealey, Dimensional scaling of cylinders in thin films of block copolymer-homopolymer ternary blends, Macromolecules **42**, 5139 (2009).

[52] J. D. Vavasour and M. D. Whitmore, Effects of solubilized homopolymer on lamellar diblock copolymer structures, Macromolecules **34**, 3471 (2001).

[53] R. J. Hickey, T. M. Gillard, M. T. Irwin, D. C. Morse, T. P. Lodge, and F. S. Bates, Phase behavior of diblock copolymer-homopolymer ternary blends: congruent first-order lamellar-disorder transition, Macromolecules **49**, 7928 (2016).

[54] M. F. Uddin, Z. Jiang, A. Raymond, A. D. Goodson, B. S. Lwoya, and J. N. L. Albert, Thin film confinement reduces compatibility in symmetric ternary block copolymer/homopolymer blends, J. Polym. Sci. B **56**, 1443 (2018).

[55] A. J. Mueller, A. P. Lindsay, A. Jayaraman, T. P. Lodge, M. K. Mahanthappa, and F. S. Bates, Emergence of a C15 laves phase in diblock polymer/homopolymer blends, ACS Macro Lett. **9**, 576 (2020).

[56] U. Jeong, D. Y. Ryu, D. H. Kho, D. H. Lee, J. K. Kim, and T. P. Russell, Phase behavior of mixtures of block copolymer and homopolymers in thin films and bulk, Macromolecules **36**, 3626 (2003).

[57] V. Mishra, S. Hur, E. W. Cochran, G. E. Stein, G. H. Fredrickson, and E. J. Kramer, Symmetry transition in thin films of diblock copolymer/homopolymer blends, Macromolecules **43**, 1942 (2010).

[58] T. A. Mykhaylyk, O. O. Mykhaylyk, S. Collins, and I. W. Hamley, Ordered structures and phase transitions in mixtures of a polystyrene/polyisoprene block copolymer with the corresponding homopolymers in thin films and in bulk, Macromolecules **37**, 3369 (2004).

[59] H. Takagi, R. Hashimoto, N. Igarashi, S. Kishimoto, and K. Yamamoto, Synchrotron SAXS studies on lattice structure of spherical micelles in binary mixtures of block copolymers and homopolymers, J. Fiber Sci. Technol. **74**, 10 (2018).

[60] H. Takagi and K. Yamamoto, Phase boundary of Frank-Kasper σ phase in phase diagrams of binary mixtures of block copolymers and homopolymers, Macromolecules **52**, 2007 (2019).

[61] M. Zhao and W. Li, Laves phases formed in the binary blend of AB4 miktoarm star copolymer and A-homopolymer, Macromolecules **52**, 1832 (2019).

[62] J. Xie and A.-C. Shi, Formation of complex spherical packing phases in diblock copolymer/homopolymer blends, Giant **5**, 100043 (2021).

[63] G. K. Cheong, F. S. Bates, and K. D. Dorfman, Symmetry breaking in particle-forming diblock polymer/homopolymer blends, Proc. Natl. Acad. Sci. USA **117**, 16764 (2020).

[64] K. D. Dorfman, Frank-Kasper phases in block polymers, Macromolecules **54**, 10251 (2021).
[65] E. L. Thomas, D. J. Kinning, D. B. Alward, and C. S. Henkee, Ordered packing arrangements of spherical micelles of diblock copolymers in two and three dimensions, Macromolecules **20**, 2934 (1987).
[66] G. E. Stein, E. J. Kramer, X. Li, and J. Wang, Layering transitions in thin films of spherical-domain block copolymers, Macromolecules **40**, 2453 (2007).
[67] J. Jung, H.-W. Park, S. Lee, H. Lee, T. Chang, K. Matsunaga, and H. Jinnai, Effect of film thickness on the phase behaviors of diblock copolymer thin film, ACS Nano **4**, 3109 (2010).
[68] J.-W. Hong, J.-H. Chang, H.-H. Hung, Y.-P. Liao, Y.-Q. Jian, I. C.-Y. Chang, T.-Y. Huang, A. Nelson, I.-M. Lin, Y.-W. Chiang *et al.*, Chain length effects of added homopolymers on the phase behavior in blend films of a symmetric, weakly segregated polystyrene-*block*-poly(methyl methacrylate), Macromolecules **55**, 2130 (2022).
[69] G. S. Doerk and K. G. Yager, Rapid ordering in "wet brush" block copolymer/homopolymer ternary blends, ACS Nano **11**, 12326 (2017).
[70] G. S. Doerk, R. Li, M. Fukuto, A. Rodriguez, and K. G. Yager, Thickness-dependent ordering kinetics in cylindrical block copolymer/homopolymer ternary blends, Macromolecules **51**, 10259 (2018).
[71] K. Toth, C. O. Osuji, K. G. Yager, and G. S. Doerk, High-throughput morphology mapping of self-assembling ternary polymer blends, RSC Adv. **10**, 42529 (2020).
[72] K. Toth, S. Bae, C. O. Osuji, K. G. Yager, and G. S. Doerk, Film thickness and composition effects in symmetric ternary block copolymer/homopolymer blend films: Domain spacing and orientation, Macromolecules **54**, 7970 (2021).
[73] G. S. Doerk, R. Li, M. Fukuto, and K. G. Yager, Wet brush homopolymers as "smart solvents" for rapid, large period block copolymer thin film self-assembly, Macromolecules **53**, 1098 (2020).
[74] P. Mahmoudi and M. W. Matsen, Entropic segregation of short polymers to the surface of a polydisperse melt, Eur. Phys. J. E **40**, 85 (2017).
[75] J. A. Hill, K. J. Endres, P. Mahmoudi, M. W. Matsen, C. Wesdemiotis, and M. D. Foster, Detection of surface enrichment driven by molecular weight disparity in virtually monodisperse polymers, ACS Macro Lett. **7**, 487 (2018).
[76] G. E. Stein, T. S. Laws, and R. Verduzco, Tailoring the attraction of polymers toward surfaces, Macromolecules **52**, 4787 (2019).
[77] S.-C. Chen, S.-W. Kuo, U.-S. Jeng, C.-J. Su, and F.-C. Chang, On modulating the phase behavior of block copolymer/homopolymer blends via hydrogen bonding, Macromolecules **43**, 1083 (2010).
[78] A. Dehghan and A.-C. Shi, Modeling hydrogen bonding in diblock copolymer/homopolymer blends, Macromolecules **46**, 5796 (2013).
[79] D. F. Sunday, A. F. Hannon, S. Tein, and R. J. Kline, Thermodynamic and morphological behavior of block copolymer blends with thermal polymer additives, Macromolecules **49**, 4898 (2016).
[80] K. Dobrosielska, S. Wakao, A. Takano, and Y. Matsushita, Nanophase-separated structures of AB block copolymer/C homopolymer blends with complementary hydrogen-bonding interactions, Macromolecules **41**, 7695 (2008).
[81] K. Dobrosielska, S. Wakao, J. Suzuki, K. Noda, A. Takano, and Y. Matsushita, Effect of homopolymer molecular weight on nanophase-separated structures of AB block copolymer/C homopolymer blends with hydrogen-bonding interactions, Macromolecules **42**, 7098 (2009).
[82] S. C. Tsai, Y. C. Lin, E. L. Lin, Y. W. Chiang, and S. W. Kuo, Hydrogen bonding strength effect on self-assembly supramolecular structures of diblock copolymer/homopolymer blends, Polym. Chem. **7**, 2395 (2016).
[83] S.-H. Tung, N. C. Kalarickal, J. W. Mays, and T. Xu, Hierarchical assemblies of block-copolymer-based supramolecules in thin films, Macromolecules **41**, 6453 (2008).
[84] A. H. Hofman, M. Reza, J. Ruokolainen, G. ten Brinke, and K. Loos, Hierarchical layer engineering using supramolecular double-comb diblock copolymers, Angew. Chem. Int. Ed. **55**, 13081 (2016).
[85] Y. Zhao, K. Thorkelsson, A. J. Mastroianni, T. Schilling, J. M. Luther, B. J. Rancatore, K. Matsunaga, H. Jinnai, Y. Wu, D. Poulsen *et al.*, Small-molecule-directed nanoparticle assembly towards stimuli-responsive nanocomposites, Nat. Mater. **8**, 979 (2009).
[86] J. Ruokolainen, R. Mäkinen, M. Torkkeli, T. Mäkelä, R. Serimaa, G. ten Brinke, and O. Ikkala, Switching supramolecular polymeric materials with multiple length scales, Science **280**, 557 (1998).
[87] W. van Zoelen, T. Asumaa, J. Ruokolainen, O. Ikkala, and G. ten Brinke, Phase behavior of solvent vapor annealed thin films of PS-*b*-P4VP(PDP) supramolecules, Macromolecules **41**, 3199 (2008).
[88] B. Nandan, M. K. Vyas, M. Böhme, and M. Stamm, Composition-dependent morphological transitions and pathways in switching of fine structure in thin films of block copolymer supramolecular assemblies, Macromolecules **43**, 2463 (2010).
[89] I. Tokarev, R. Krenek, Y. Burkov, D. Schmeisser, A. Sidorenko, S. Minko, and M. Stamm, Microphase separation in thin films of poly(styrene-*block*-4-vinylpyridine) copolymer-2-(4′-hydroxybenzeneazo)benzoic acid assembly, Macromolecules **38**, 507 (2005).
[90] M. W. Matsen, Immiscibility of large and small symmetric diblock copolymers, J. Chem. Phys. **103**, 3268 (1995).
[91] L. D. Williamson and P. F. Nealey, Macrophase separation of blends of diblock copolymers in thin films, Macromolecules **48**, 3997 (2015).
[92] K. G. Yager, E. Lai, and C. T. Black, Self-assembled phases of block copolymer blend thin films, ACS Nano **8**, 10582 (2014).
[93] K. Kremer and G. S. Grest, Dynamics of entangled linear polymer melts: A molecular-dynamics simulation, J. Chem. Phys. **92**, 5057 (1990).
[94] G. S. Grest, M. Lacasse, K. Kremer, and A. M. Gupta, Efficient continuum model for simulating polymer blends and copolymers, J. Chem. Phys. **105**, 10583 (1996).
[95] C. Forrey, K. G. Yager, and S. P. Broadaway, Molecular dynamics study of the role of the free surface on block copolymer thin film morphology and alignment, ACS Nano **5**, 2895 (2011).

[96] S. Bae and K. G. Yager, Chain redistribution stabilizes coexistence phases in block copolymer blends, ACS Nano **16**, 17107 (2022).

[97] S. Bae, M. M. Noack, and K. G. Yager, Surface enrichment dictates block copolymer orientation, Nanoscale **15**, 6901 (2023).

[98] S. T. Russell, S. Bae, A. Subramanian, N. Tiwale, G. Doerk, C.-Y. Nam, M. Fukuto, and K. G. Yager, Priming self-assembly pathways by stacking block copolymers, Nat. Commun. **13**, 6947 (2022).

[99] G. S. Doerk, A. Stein, S. Bae, M. M. Noack, M. Fukuto, and K. G. Yager, Autonomous discovery of emergent morphologies in directed self-assembly of block copolymer blends, Sci. Adv. **9**, eadd3687 (2023).

[100] S. R. Nowak, N. Tiwale, G. S. Doerk, C.-Y. Nam, C. T. Black, and K. G. Yager, Responsive blends of block copolymers stabilize the hexagonally perforated lamellae morphology, Soft Matter **19**, 2594 (2023).

[101] W. I. Park, Y. Kim, J. W. Jeong, K. Kim, J.-K. Yoo, Y. H. Hur, J. M. Kim, E. L. Thomas, A. Alexander-Katz, and Y. S. Jung, Host-guest self-assembly in block copolymer blends, Sci. Rep. **3**, 3190 (2013).

[102] D. S. Jung, J. Bang, T. W. Park, S. H. Lee, Y. K. Jung, M. Byun, Y.-R. Cho, K. H. Kim, G. H. Seong, and W. I. Park, Pattern formation of metal-oxide hybrid nanostructures via the self-assembly of di-block copolymer blends, Nanoscale **11**, 18559 (2019).

[103] M. Byun, T. W. Park, and W. I. Park, Hierarchically ordered hybrid nanostructures via spontaneous self-assembly of block copolymer blends, Thin. Solid. Films **701**, 137928 (2020).

[104] V. Pryamitsyn, S. H. Han, J. K. Kim, and V. Ganesan, Curvature modification of block copolymer microdomains using blends of block copolymers with hydrogen bonding interactions, Macromolecules **45**, 8729 (2012).

[105] S. H. Han, V. Pryamitsyn, D. Bae, J. Kwak, V. Ganesan, and J. K. Kim, Highly asymmetric lamellar nanopatterns via block copolymer blends capable of hydrogen bonding, ACS Nano **6**, 7966 (2012).

[106] C. Tang, E. M. Lennon, G. H. Fredrickson, E. J. Kramer, and C. J. Hawker, Evolution of block copolymer lithography to highly ordered square arrays, Science **322**, 429 (2008).

[107] C. Tang, S. Hur, B. C. Stahl, K. Sivanandan, M. Dimitriou, E. Pressly, G. H. Fredrickson, E. J. Kramer, and C. J. Hawker, Thin film morphology of block copolymer blends with tunable supramolecular interactions for lithographic applications, Macromolecules **43**, 2880 (2010).

[108] S. Kang, J. Lee, E. Kim, Y. Seo, C. Choi, and J. K. Kim, Inverted cylindrical microdomains from binary block copolymer blends capable of hydrogen bonding, Macromolecules **54**, 8971 (2021).

[109] Y.-H. Ting, S.-M. Park, C.-C. Liu, X. Liu, F. J. Himpsel, P. F. Nealey, and A. E. Wendt, Plasma etch removal of poly(methyl methacrylate) in block copolymer lithography, J. Vac. Sci. Technol. B **26**, 1684 (2008).

[110] T. Thurn-Albrecht, R. Steiner, J. DeRouchey, C. M. Stafford, E. Huang, M. Bal, M. Tuominen, C. J. Hawker, and T. P. Russell, Nanoscopic templates from oriented block copolymer films, Adv. Mater. **12**, 787 (2000).

[111] A. S. Zalusky, R. Olayo-Valles, J. H. Wolf, and M. A. Hillmyer, Ordered nanoporous polymers from polystyrene−polylactide block copolymers, J. Am. Chem. Soc. **124**, 12761 (2002).

[112] S. Park, B. Kim, J.-Y. Wang, and T. P. Russell, Fabrication of highly ordered silicon oxide dots and stripes from block copolymer thin films, Adv. Mater. **20**, 681 (2008).

[113] X. Gu, I. Gunkel, and T. P. Russell, Pattern transfer using block copolymers, Philos. Trans. R. Soc. A **371**, 20120306 (2013).

[114] Y. S. Jung and C. A. Ross, Orientation-controlled self-assembled nanolithography using a polystyrene-polydimethylsiloxane block copolymer, Nano Lett. **7**, 2046 (2007).

[115] C. M. Bates, J. R. Strahan, L. J. Santos, B. K. Mueller, B. O. Bamgbade, J. A. Lee, J. M. Katzenstein, C. J. Ellison, C. G. Willson, T. Seshimo *et al.*, Polarity-switching top coats enable orientation of sub-10-nm block copolymer domains, Science **338**, 775 (2012).

[116] J. Chai and J. M. Buriak, Using cylindrical domains of block copolymers to self-assemble and align metallic nanowires, ACS Nano **2**, 489 (2008).

[117] A. Subramanian, N. Tiwale, G. Doerk, K. Kisslinger, and C.-Y. Nam, Enhanced hybridization and nanopatterning via heated liquid-phase infiltration into self-assembled block copolymer thin films, ACS Appl. Mater. Interfaces **12**, 1444 (2020).

[118] M. Ma, R. Liu, T. Su, Z. Sun, and C. A. Ross, Reversible morphology locking via metal infiltration in a block copolymer, ACS Nano **17**, 12225 (2023).

[119] Q. Peng, Y.-C. Tseng, S. B. Darling, and J. W. Elam, Nanoscopic patterned materials with tunable dimensions via atomic layer deposition on block copolymers, Adv. Mater. **22**, 5129 (2010).

[120] Q. Peng, Y.-C. Tseng, S. B. Darling, and J. W. Elam, A route to nanoscopic materials via sequential infiltration synthesis on block copolymer templates, ACS Nano **5**, 4600 (2011).

[121] A. Subramanian, G. Doerk, K. Kisslinger, D. H. Yi, R. B. Grubbs, and C.-Y. Nam, Three-dimensional electroactive ZnO nanomesh directly derived from hierarchically self-assembled block copolymer thin films, Nanoscale **11**, 9533 (2019).

[122] S. Lee, A. Subramanian, N. Tiwale, K. Kisslinger, M. Mumtaz, L.-Y. Shi, K. Aissou, C.-Y. Nam, and C. A. Ross, Resolving triblock terpolymer morphologies by vapor-phase infiltration, Chem. Mater. **32**, 5309 (2020).

[123] D. Nowak, W. Morrison, H. K. Wickramasinghe, J. Jahng, E. Potma, L. Wan, R. Ruiz, T. R. Albrecht, K. Schmidt, J. Frommer *et al.*, Nanoscale chemical imaging by photoinduced force microscopy, Sci. Adv. **2**, e1501571 (2016).

[124] S. Akkineni, G. S. Doerk, C. Shi, B. Jin, S. Zhang, S. Habelitz, and J. J. De Yoreo, Biomimetic mineral synthesis by nanopatterned supramolecular-block copolymer templates, Nano Lett. **23**, 4290 (2023).

[125] C. M. Stafford, K. E. Roskov, T. H. Epps, and M. J. Fasolka, Generating thickness gradients of thin polymer films via flow coating, Rev. Sci. Instrum. **77**, 023908 (2006).

[126] R. L. Davis, S. Jayaraman, P. M. Chaikin, and R. A. Register, Creating controlled thickness gradients in polymer thin films via flowcoating, Langmuir **30**, 5637 (2014).

[127] A. P. Smith, J. F. Douglas, J. C. Meredith, E. J. Amis, and A. Karim, Combinatorial study of surface pattern formation in thin block copolymer films, Phys. Rev. Lett. **87**, 015503 (2001).

[128] J. C. Meredith, A. Karim, and E. J. Amis, Combinatorial methods for investigations in polymer materials science, MRS Bull. **27**, 330 (2002).

[129] S. V. Roberson, A. J. Fahey, A. Sehgal, and A. Karim, Multifunctional ToF-SIMS: Combinatorial mapping of gradient energy substrates, Appl. Surf. Sci. **200**, 150 (2002).

[130] A. P. Smith, A. Sehgal, J. F. Douglas, A. Karim, and E. J. Amis, Combinatorial mapping of surface energy effects on diblock copolymer thin film ordering, Macromol. Rapid Commun. **24**, 131 (2003).

[131] J. N. L. Albert, M. J. Baney, C. M. Stafford, J. Y. Kelly, and T. H. I. Epps, Generation of monolayer gradients in surface energy and surface chemistry for block copolymer thin film studies, ACS Nano **3**, 3977 (2009).

[132] J. C. Meredith, A. P. Smith, A. Karim, and E. J. Amis, Combinatorial materials science for polymer thin-film dewetting, Macromolecules **33**, 9747 (2000).

[133] J. N. L. Albert, T. D. Bogart, R. L. Lewis, K. L. Beers, M. J. Fasolka, J. B. Hutchison, B. D. Vogt, and T. H. I. Epps, Gradient solvent vapor annealing of block copolymer thin films using a microfluidic mixing device, Nano Lett. **11**, 1351 (2011).

[134] J. C. Meredith, A. Karim, and E. J. Amis, High-throughput measurement of polymer blend phase behavior, Macromolecules **33**, 5760 (2000).

[135] X. Rodríguez-Martínez, S. Sevim, X. Xu, C. Franco, P. Pamies-Puig, L. Córcoles-Guija, R. Rodriguez-Trujillo, F. J. del Campo, D. Rodriguez San Miguel, A. J. deMello *et al.*, Microfluidic-assisted blade coating of compositional libraries for combinatorial applications: The case of organic photovoltaics, Adv. Energy Mater. **10**, 2001308 (2020).

[136] A. L. Liu, E. M. Dogan-Guner, M. McBride, R. Venkatesh, M. A. Gonzalez, E. Reichmanis, M. Grover, and J. C. Meredith, Composition gradient high-throughput polymer libraries enabled by passive mixing and elevated temperature operability, Chem. Mater. **34**, 6659 (2022).

[137] E. J. Kluender, J. L. Hedrick, K. A. Brown, R. Rao, B. Meckes, J. S. Du, L. M. Moreau, B. Maruyama, and C. A. Mirkin, Catalyst discovery through megalibraries of nanomaterials, Proc. Natl. Acad. Sci. USA **116**, 40 (2019).

[138] K. Toth, C. O. Osuji, K. G. Yager, and G. S. Doerk, Electrospray deposition tool: Creating compositionally gradient libraries of nanomaterials, Rev. Sci. Instrum. **91**, 013701 (2020).

[139] H. S. Stein and J. M. Gregoire, Progress and prospects for accelerating materials science with automated and autonomous workflows, Chem. Sci. **10**, 9640 (2019).

[140] E. Stach, B. DeCost, A. G. Kusne, J. Hattrick-Simpers, K. A. Brown, K. G. Reyes, J. Schrier, S. Billinge, T. Buonassisi, I. Foster *et al.*, Autonomous experimentation systems for materials development: A community perspective, Matter **4**, 2702 (2021).

[141] M. Abolhasani and E. Kumacheva, The rise of self-driving labs in chemical and materials sciences, Nat. Synth **2**, 483 (2023).

[142] M. M. Noack, K. G. Yager, M. Fukuto, G. S. Doerk, R. Li, and J. A. Sethian, A kriging-based approach to autonomous experimentation with applications to x-ray scattering, Sci. Rep. **9**, 11809 (2019).

[143] M. M. Noack, G. S. Doerk, R. Li, M. Fukuto, and K. G. Yager, Advances in kriging-based autonomous x-ray scattering experiments, Sci. Rep. **10**, 1325 (2020).

[144] M. M. Noack, G. S. Doerk, R. Li, J. K. Streit, R. A. Vaia, K. G. Yager, and M. Fukuto, Autonomous materials discovery driven by Gaussian process regression with inhomogeneous measurement noise and anisotropic kernels, Sci. Rep. **10**, 17663 (2020).

[145] M. M. Noack, P. H. Zwart, D. M. Ushizima, M. Fukuto, K. G. Yager, K. C. Elbert, C. B. Murray, A. Stein, G. S. Doerk, E. H. R. Tsai *et al.*, Gaussian processes for autonomous data acquisition at large-scale synchrotron and neutron facilities, Nat. Rev. Phys. **3**, 685 (2021).

[146] K. G. Yager, P. W. Majewski, M. M. Noack, and M. Fukuto, Autonomous x-ray scattering, Nanotechnology **34**, 322001 (2023).

[147] A. Stein, G. Wright, K. G. Yager, G. S. Doerk, and C. T. Black, Selective directed self-assembly of coexisting morphologies using block copolymer blends, Nat. Commun. **7**, 12366 (2016).

[148] P. W. Majewski and K. G. Yager, Millisecond ordering of block copolymer films via photothermal gradients, ACS Nano **9**, 3896 (2015).

[149] P. W. Majewski and K. G. Yager, Block copolymer response to photothermal stress fields, Macromolecules **48**, 4591 (2015).

[150] S. R. Nowak and K. G. Yager, Photothermally directed assembly of block copolymers, Adv. Mater. Interfaces **7**, 1901679 (2020).

[151] P. W. Majewski, A. Rahman, C. T. Black, and K. G. Yager, Arbitrary lattice symmetries via block copolymer nanomeshes, Nat. Commun. **6**, 7448 (2015).

[152] A. Rahman, P. W. Majewski, G. Doerk, C. T. Black, and K. G. Yager, Non-native three-dimensional block copolymer morphologies, Nat. Commun. **7**, 13988 (2016).

[153] C. Shin, H. Ahn, E. Kim, D. Y. Ryu, J. Huh, K. W. Kim, and T. P. Russell, Transition behavior of block copolymer thin films on preferential surfaces, Macromolecules **41**, 9140 (2008).

[154] E. Kim, S. Choi, R. Guo, D. Y. Ryu, C. J. Hawker, and T. P. Russell, Transition behavior of PS-*b*-PMMA films on the balanced interfacial interactions, Polymer **51**, 6313 (2010).

[155] Y. Kim, D. Yong, W. Lee, H. Ahn, J. H. Kim, J. U. Kim, and D. Y. Ryu, Order-to-disorder transition of lamella-forming PS-*b*-P2VP films confined between the preferential surface and neutral substrate, Macromolecules **52**, 8672 (2019).

[156] D. F. Sunday, J. L. Thelen, C. Zhou, J. Ren, Paul. F. Nealey, and R. J. Kline, Buried structure in block copolymer films revealed by soft x-ray reflectivity, ACS Nano **15**, 9577 (2021).

[157] P. W. Majewski and K. G. Yager, Latent alignment in pathway-dependent ordering of block copolymer thin films, Nano Lett. **15**, 5221 (2015).

[158] Y. Choo, P. W. Majewski, M. Fukuto, C. O. Osuji, and K. G. Yager, Pathway-engineering for highly-aligned block copolymer arrays, Nanoscale **10**, 416 (2018).

[159] Y. Sun, R. Tan, Z. Ma, Z. Gan, G. Li, D. Zhou, Y. Shao, W.-B. Zhang, R. Zhang, and X.-H. Dong, Discrete block copolymers with diverse architectures: Resolving complex spherical phases with one monomer resolution, ACS Cent. Sci. **6**, 1386 (2020).

[160] H. Feng, M. Dolejsi, N. Zhu, S. Yim, W. Loo, P. Ma, C. Zhou, G. S. W. Craig, W. Chen, L. Wan *et al.*, Optimized design of

block copolymers with covarying properties for nanolithography, Nat. Mater. **21**, 1426 (2022).

[161] W. S. Loo, H. Feng, T. J. Ferron, R. Ruiz, D. F. Sunday, and P. F. Nealey, Determining structure and thermodynamics of A-*b*−(B-*r*-C) copolymers, ACS Macro Lett. **12**, 118 (2023).

[162] A. J. DeStefano, R. A. Segalman, and E. C. Davidson, Where biology and traditional polymers meet: The potential of associating sequence-defined polymers for materials science, JACS Au **1**, 1556 (2021).

[163] A. L. Patterson, S. P. O. Danielsen, B. Yu, E. C. Davidson, G. H. Fredrickson, and R. A. Segalman, Sequence effects on block copolymer self-assembly through tuning chain conformation and segregation strength utilizing sequence-defined polypeptoids, Macromolecules **52**, 1277 (2019).

[164] A. L. Patterson, B. Yu, S. P. O. Danielsen, E. C. Davidson, G. H. Fredrickson, and R. A. Segalman, Monomer sequence effects on interfacial width and mixing in self-assembled diblock copolymers, Macromolecules **53**, 3262 (2020).